ANA LAURA LORDI DIAS

SEISMIC SEQUENCES INDUCED BY WATER LOADS IN AZORES

UNIVERSIDADE DO ALGARVE

FACULDADE DE CIÊNCIAS E TECNOLOGIA

2021

ANA LAURA LORDI DIAS

SEISMIC SEQUENCES INDUCED BY WATER LOADS IN AZORES

Master in Marine and Coastal Systems

Work performed under the supervision of:
Dr. Maria Conceição Neves (Universidade do Algarve)
Dr. Susana Custódio (Universidade de Lisboa)

UNIVERSIDADE DO ALGARVE

FACULDADE DE CIÊNCIAS E TECNOLOGIA

2021

SEISMIC SEQUENCES INDUCED BY WATER LOADS IN AZORES

Declaração de Autoria do Trabalho

Declaro ser o(a) autor(a) deste trabalho, que é original e inédito. Autores e trabalhos consultados estão devidamente citados no texto e constam da listagem de referências incluída.

Declaration of Authorship of work

I declare to be the author of this work, which is original and unpublished. Authors and works consulted are duly cited in the text and are included in the list of references.

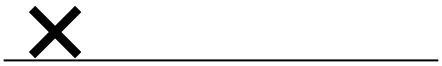

Ana Laura Lordi Dias

ACKNOWLEDGMENTS

I would like to thank God for this amazing opportunity and my parents Ana Paula and Cassio and my sister Maria Julia for all support, opportunities and unconditional love you always gave it to me, mainly during these two years of study in Portugal.

Thanks to my grandparents for always putting me in their prayers.

To my boyfriend and best friend, Matheus, I appreciate all the love, strength, and companionship over these years we were so far away from each other.

Thank you to my supervisors Dr. Maria Conceição Neves and Dr. Susana Custódio who introduced me the subject of this work. Thank you for all support and patience throughout this study. I have gained unvaluable experience and knowledge from you.

Thank you to all the professors of this master course, it was a pleasure to learn from you.

Thank you to my brazilian flatmates for all advices and long conversations we had. It was a pleasure to share the house with you.

To my friends and collegues from this master course, Catherine, Jacque, Bruno, Rachel, Sarah, and others, I wish you all the best for your careers, it was a pleasure to learn alongside you. Thank you for the great time and dinners we had together. I really enjoyed meeting you all, and I hope we meet again soon.

RESUMO

Em diversas partes do mundo já foi observado o aumento da taxa de sismicidade associada aos efeitos de cargas hidrológicas na crosta (Bollinger et al. 2007; Craig et al. 2017; Dumont et al. 2020). Desta forma, este trabalho investiga a conexão entre cargas atmosféricas e hidrológicas e a deformação crustal na região dos Açores, procurando por modulações sazonais e inter-anuais na taxa de ocorrência de sismos, que podem ser causadas pela variação atmosférica e hidrológica. O presente estudo envolve a manipulação e o *declustering* do catálogo sísmico dos Açores, de 2008 a 2018 e uma análise estatística dos dados. A metodologia utilizada nos dados dos Açores foi primeiro testada no sistema de falhas de Nova Madrid (EUA), seguindo o artigo de Craig et al. 2017, onde foi descoberta uma conexão entre o aumento da sismicidade e a baixa taxa de chuva no final do Verão. Isto ocorre, pois durante o Inverno, a carga hidrológica do rio Mississippi que é cortado pelo sistema de falhas exerce pressão sobre a crosta. Durante o Verão, a crosta soergue devido ao alívio de carga e então desencadeia uma alta atividade sísmica. Os resultados obtidos neste trabalho se mostraram compatíveis aos resultados encontrados pelo autor. Sendo assim, a metodologia utilizada foi aplicada aos Açores. A análise dos dados dos Açores foi realizada separadamente, para a região oceânica e para as ilhas, já que diferentes processos físicos ocorrem em ambos locais. As ilhas sofrem com as marés terrestres, precipitação e variação nas águas subterrâneas, enquanto o oceano sofre com o peso da coluna d'água. Assim, de forma a analisar melhor a sazonalidade e os possíveis mecanismos atuantes, o catálogo foi divido. A janela temporal dos dados (de 2008 a 2018) foi escolhida de forma que mudanças nas redes sísmicas e trocas de equipamento não afetassem os dados. O primeiro passo neste estudo foi eliminar eventos sísmicos dependentes de um evento principal, através de um processo chamado *declustering*, de modo que apenas restasse os eventos independentes, chamados de *mainshocks*. O *declustering* é essencial na análise de sazonalidade dos dados, já que eventos dependentes poderiam tendenciar os dados. Antes da análise de sazonalidade, foi calculada a razão entre o número de eventos que ocorrem nos meses de Inverno e aqueles que ocorrem nos meses de Verão. Esta razão mostrou que mais eventos estavam ocorrendo no Verão quando comparados com o período de Inverno. Na análise de sazonalidade foram empregues métodos estatísticos como a simulação de Monte Carlo e a abordagem *Jack-Knife*. A simulação de Monte Carlo foi utilizada para gerar 10 mil catálogos aleatórios baseados nos catálogos originais. A razão Inverno/Verão de cada um dos 10 mil catálogos foi calculada assim como os

intervalos de confiança de 99% e 95%, com a finalidade de se observar uma razão Inverno/Verão ao acaso semelhante à razão observada. Os resultados desta análise mostraram que para a sismicidade oceânica, considerando os intervalos de magnitude de 2.0 a 2.7 e de 3.5 a 4.8, a probabilidade de se observar a mesma razão Inverno/Verão é menor que 1%, confirmando que a sazonalidade é genuína. Já para as ilhas, a razão Inverno/Verão caiu dentro dos intervalos de confiança, o que indica que a sazonalidade está ocorrendo por acaso. A abordagem de *Jack-Knife*, foi realizada para confirmar os resultados obtidos na simulação. Durante esta etapa, todo o processo anterior de geração dos 10 mil catálogos e cálculo das razões é repetido, mas agora removendo ano a ano dos dados, um de cada vez. Esta abordagem permite identificar eventos climáticos extremos que podem ter ocorrido durante os anos e interferiram na sazonalidade. Não foram encontrados eventos anômalos para região oceânica, confirmando que ao longo de 11 anos a sazonalidade se mostrou genuína. Sendo assim, a taxa sísmica oceânica mensal foi calculada e comparada com as séries temporais mensais de precipitação, altura total das ondas, pressão atmosférica e pressão média ao nível do mar. As componentes principais que mais contribuem para cada série temporal foram escolhidas durante a Análise Espectral Singular, que decompõe e reconstrói os sinais das séries, em seguida correlacionadas com as componentes principais da taxa sísmica. Os resultados da correlação mostraram que a taxa sísmica oceânica está correlacionada negativamente com a taxa de precipitação por um coeficiente de correlação de -0.69, por -0.77 com a altura total das ondas, e positivamente com a pressão atmosférica (0.40) e com a pressão a nível do mar (0.39). Em sequência, foi realizado o teste de *t-student*, que confirmou que os resultados da correlação são significativos. Os resultados deste estudo demonstram que a modulação sazonal da taxa de sismicidade oceânica é presente em cada ano (de 2008 a 2018). Assim como no sistema de falhas de Nova Madrid, a taxa de sismicidade oceânica dos Açores é maior durante o Verão (nos meses de J-A-S-O) e menor durante o Inverno (nos meses de J-F-M-A). Estudos futuros devem focar em quantificar as tensões causadas pelas cargas hidrológicas mencionadas, a fim de que se confirme a influência delas na sismicidade, além de investigar outros possíveis mecanismos, como as marés. Os resultados fornecem uma avaliação de variações cíclicas na sismicidade e sua relação com perturbações hidrológicas e atmosféricas na região dos Açores. Além disso, proporciona uma primeira abordagem da precipitação e da altura total das ondas como possíveis mecanismos de desencadeamento da atividade sísmica oceânica na região, contribuindo para melhorar a nossa compreensão sobre os

mecanismos de desencadeamento dos sismos em sistemas vulcano-tectônicos ativos e para a previsão de períodos onde há aumento da sismicidade.

Palavras-chave: Sismicidade; Cargas hidrológicas; Modulação Sazonal; Açores

ABSTRACT

This work investigates the connection between atmospheric and hydrological loads and crustal deformation in the Azores region, looking in particular for seasonal and inter-annual modulations of the earthquake occurrence rate which can be caused by atmospheric and hydrological variations. The work involves the manipulation and declustering of the Azores seismic catalogue, from 2008 to 2018, and statistical analysis of the data. The New Madrid Seismic Zone (NMSZ, USA), where a connection between enhanced seismicity and low rainfall rate in late summer had already been recognized, is used as a benchmark study site to test the methodology. The analysis of the Azores data was carried out separately, for the oceanic region and for the islands, and also considering earthquakes with magnitude above 2.0 (the magnitude of completeness). Just as for the NMSZ, the oceanic seismicity rate of the Azores is higher during Summer/fall (J-A-S-O months) and lower during Winter/Spring (J-F-M-A months). Monte Carlo simulations, used to check if the seasonal and inter-annual variations found in the seismicity pattern are statistically significant and not observed by chance, show that the probability of observing such seasonality by chance is less than 1% for magnitude bands from 2.0 to 2.7 and from 3.8 to 4.5. The influence of extreme climatic events is investigated using a Jack-knife approach. The results demonstrate that the seasonal modulation of the ocean seismicity rate is present at each calendar year (from 2008 to 2018) and is not the consequence of single extreme climatic deviations. Unlike the ocean region, where the seasonality is more evident and genuine in both catalogues, the islands presented a seasonality that was statistically genuine only in the full catalogue. The study of the seasonal modulation investigated using methods of decomposition and reconstruction of geophysical time series (SSA – Singular Spectrum Analysis) show that the principal components of the Azores ocean seismicity rate is negatively correlated with the principal components of rainfall (-0.69) and the significant height of wind waves and swell (-0.77) and positively correlated with atmospheric pressure (0.40) and mean sea level pressure (0.39). The results provide a first assessment of cyclic variations in seismicity and its relationship with atmospheric and hydrological disturbances in the Azores region.

Key-words: Seismicity; Hydrological loads; Seasonal modulations; Azores

LIST OF FIGURES

LIST OF TABLES

TABLE OF CONTENTS

1 INTRODUCTION

Seismic activity is caused by elastic stresses in the lithosphere, which is in constant deformation. When the stresses acting on a fault reach a critical level, an earthquake occurs. Several factors can change the stress state of active faults and trigger earthquakes, such as climate events causing changes in atmospheric pressure, volcanic eruptions, and hydrologic loads.

Hydrological loadings such as snow, precipitation, tides, and groundwater have been suggested in many studies to modulate the seismicity of active tectonic sites. These may contribute to strain and stress transients that trigger small earthquake swarms at faults that are already near failure, as widely demonstrated by stress triggering studies (Stein 1999; Heki 2003; Do Nascimento et al. 2004; Gahalaut et al. 2007; Brothers et al. 2011; Neves et al. 2015, Dumont et al. 2020). Two mechanisms have been suggested by which hydrological loadings influence earthquake occurrences. The stresses are either induced directly on the fault systems or via pore-fluid pressure, but in some cases, it is not clear which process is in action.

During wet periods, the hydrological load variation causes pressure and deforms the crust. When the water load is released, the crust, which has an elastic behavior, tends to go back to its original position (isostatic movement). During the rebound process, the faults can be activated and generate microearthquakes (Heki 2003; Bollinger et al. 2007; Craig et al. 2017; Ueda and Kato 2019; Dumont et al. 2020).

The magnitude of the hydrologically derived variations in stress is small (of the order of few kPa) compared with the long-term tectonic stresses, therefore it is necessary to look for changes in the background state of stress, that can be revealed by seasonal and inter-annual modulations of the earthquake occurrence rate. This requires the manipulation of seismic catalogues and the use of statistical methods to check if the seasonal and inter-annual variations are statistically significant, and not the result of extreme climatic events.

The present work focuses on how annual and multi-annual stress changes of atmospheric and hydrological origin may affect the generation of seismic sequences on the Azores, characterized by intense seismic activity of both tectonic and volcanic origin. A similar study conducted in the New Madrid Seismic Zone in USA (Craig et al. 2017) is used as a benchmark to test the

methodology. Because these processes are periodic, the first part of the study focuses on identifying the hydrological seasonal patterns and the second part on analyzing its correlation with seismicity rate.

This work provides an assessment of cyclic variations in seismicity and its relationship with atmospheric disturbances and hydrologically-driven load in the Azores region. Since microearthquakes might be a trigger for higher magnitude earthquakes it contributes to improving our understanding of the physics of earthquake triggering processes.

1.1 OBJECTIVE

The main objective of this work is to study if the seismicity of the Azores is being influenced by hydrologic and atmospheric loadings, that are possible drivers of the seismic activity in the area, facilitating mainshock occurrences. This study aims to contribute to a better understanding of the seismicity triggers in an active volcano-tectonic system.

2 THE STATE OF THE ART REVIEW

In the past few years, many studies have observed a correlation between seasonal variations in the number of earthquakes and hydrological cycles in several places worldwide. The hydrological loads such as rain, snow and tides were suggested as possible mechanisms that help to enhance the seismic activity in these areas. The major studies are set out below.

The analysis of the shear stress change of the faults by Heki (2003) evidenced that the snow load in the Japanese Islands causes seasonal crust deformation inland, since it enhances the compression (negative stress change) on reverse faults and disturbs the interseismic strain buildup. Heki (2003) showed that the compression caused by the snow on the crust was larger than 5 kPa, as shown in Figure 1.

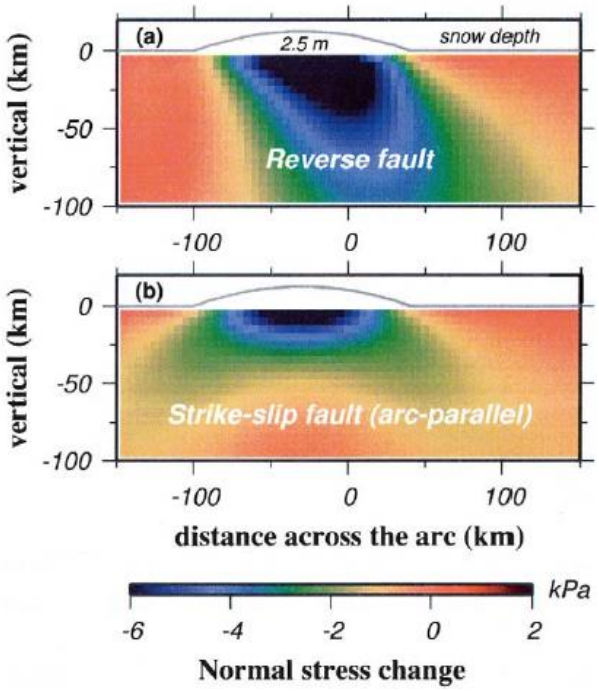

Figure 1. Cross-section of negative changes in normal stress (compression) at a reverse **(a)** and a strike-slip fault **(b)**. The snow depth curve is shown above the ground at a maximum depth of 2.5 m at 330 km (from Heki, 2003).

In Nepal, seasonal variations of snow loading as well as precipitation and variations of the water table were observed in the Himalayas. Bollinger et al. 2007 showed that the absence of

earthquakes in the summer, caused by stress-loading, follows the monsoon rains in the Ganges River and northern India, as shown in the histogram of Figure 2. The methodology used by the authors involves the declustering method to overcome the contamination of the data caused by aftershocks, which can mask seasonality. In addition, the statistical significance of the observations was tested generating random catalogues. The same approach is going to be used and explained further in this work.

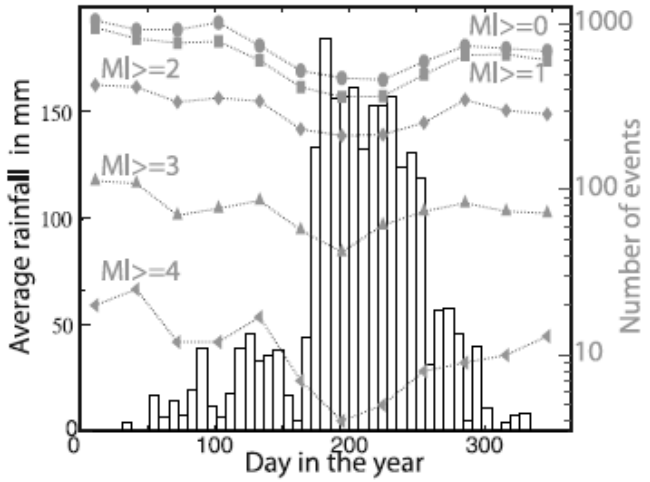

Figure 2. Eight-day averages for rainfall for 1998 (vertical bars), compared to monthly averages for numbers of earthquakes in different magnitude ranges (symbols) averaged over the period range 1995 to 2000. Maximum precipitation corresponds to minimum earthquake activity in all magnitude bands (from Bollinger et al. 2007).

Another example of how hydrological loadings interfere in the seismicity is given by Ueda & Kato 2019, who proposed that the increase of the pore pressure within fault zones caused by heavy precipitation in autumn and snow melting in spring might be plausible mechanisms, since they lead to the weakening of the fault strength and increase the seismicity in these months in San-in District (Japan). The authors suggested that the seismicity rate in San-in District has been related to seasonal patterns for at least 150 years. In their study, a new approach was used to evaluate the significance of the seasonal variations. According to the authors, uncertainties derived from a declustering method, which have been rarely considered in previous studies should be incorporated into the evaluation of seasonal modulation of seismicity. Therefore, the

authors used a probability-based declustering procedure, adopting uncertainties derived from the declustering method.

Not only does the rain and snow load interfere in the seismicity, but also the ocean load. At long timescales (thousands of years) Neves et al. 2015 evidenced for the Portuguese territory that the stresses caused by changes in sea level (of the order of MPa) can impact faults, promoting or inhibiting failure depending on fault type, depth and distance to the coastline. At shorter time scales, ocean tides also play a role in the seismic activity, but in this case, the load exerted on the crust is smaller, of the order of kPa. Tanaka 2014 highlights that the statistical probability of earthquake occurrence may change over a day, due to periodic variations in the tidal stress acting on faults.

Craig et al. 2017 identified variations in the rate of microearthquakes in the intraplate New Madrid Seismic Zone (NMSZ) at annual and multi-annual timescales, coinciding with hydrological loading in the upper Mississippi embayment, USA. They applied the same approach used by Bollinger et al. 2007 to test the statistical significance of the data (the generation of random catalogues). The correlation analysis between the hydrological load of Mississippi and the microearthquakes was based on GPS displacement data series, that monitors the surface displacements of the NMSZ; satellite gravity measurements (from GRACE), and the Mississippi River stage (Figure 3).

The investigation of Craig et al. 2017 found an anti-correlation between seismicity and river stage and between seismicity and GRACE-observed loading, that is, maximum seismicity correspondents to minimum load, at both annual and multi-annual timescales.

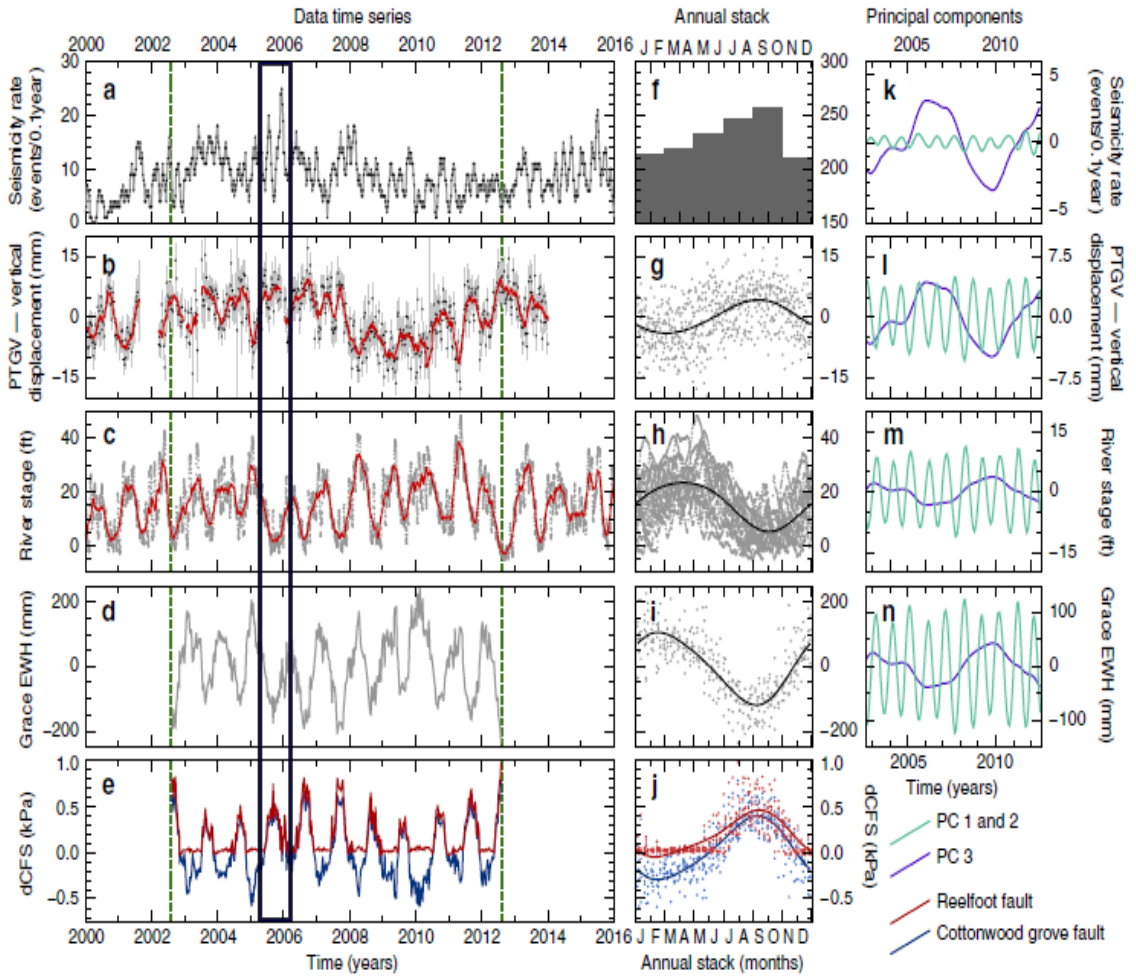

Figure 3. (a) Relationship between seismicity rate in Reelfoot fault, NMSZ, **(b)** GPS displacements, **(c)** river stage observations, **(d)** GRACE gravity observations, **(e)** calculated Coulomb failure stress variations from GRACE loading variations for the Reelfoot fault (red) and Cottonwood grove fault (blue**), (f)** is the earthquake frequency histogram, stacked on an annual timescale, **g–j** as in **b–e,** but stacked on an annual timescale**.** Curves are a best-fit four-component annual Fourier series to the stacked data, and **k–n** is the first three principal components for seismicity rate, GPS displacement, river stage and GRACE gravity, respectively, as determined from Multi-channel Singular Spectrum**.** The black rectangle represents the correlation between the seismicity, GPS displacements and the Coulomb stress (enhanced during seismicity), and the anti-correlation where the minimum river stage, and GRACE load variations corresponds to maximum seismicity (Modified from Craig et al. 2017).

Regarding the two mechanisms aforementioned that had been suggested by which hydrological loadings can influence the earthquake occurrence, Craig et al. 2017 argued that an inverse correlation at multiple periods allows to rule out a pore-fluid pressure-related effect, since the

observed variation in seismicity rates of the NMSZ appears to be approximately in phase with the stresses resulting from the variation in surface loading, at annual and longer periods. Therefore, the seismicity rate in NMSZ was considered driven directly by changes in elastic stresses acting on the fault system, and not influenced by pore-fluid pressure variations (in which the seismicity rate should be delayed relative to the hydrological load).

In 2018, Kreemer & Zaliapin found in California a correlation between seasonal variations in seismicity and horizontal dilatational strain. The authors used horizontal seasonal GPS displacements and converted it into a strain field. They inferred that the hydrological loading is likely the main driver of the observed horizontal strain in the northern part of the area.

The results of the work suggest that the seasonal deformation correlates with the proportion of large earthquakes and shows an anticorrelation with the aftershock production. So even though seasonal deformation may not directly trigger earthquakes, if an earthquake happens during the right season, it seems to be able to grow a little larger, releasing a little more stress than it otherwise would and reducing the need for (more) aftershocks (Kreemer & Zaliapin 2018).

In the Azores, Martini et al. 2009 used seismic velocities to point that a seasonal effect occurs in the seismicity rate around the Fogo Massif, in São Miguel island. Their results show a seasonal cycle of the velocity patterns, where lower velocities appear in wintertime related to high rainfall, and higher velocities in summer related to low rainfall. According to Martini et al. 2009, the annual periodicity of the rainfall and the seismicity appear to be the same, which indicates that the rain is helping to drive the seismicity. Besides, the seismicity in São Miguel seems to occur preferably in periods of more abundant rainfall.

Overall, the mentioned studies observed that in some tectonic sites the absence of seismicity might be positively correlated with the rainfall, such as in São Miguel Island, and in other sites, it might be negatively correlated, such as in New Madrid Seismic Zone. In the latter case, the variation in the seismicity rate is a result of direct stress effects on the fault system. In the former case, the variations in the seismicity rate might be related to local pressure changes at depth in response to the water load.

The studies aforementioned showed that in several places around the world hydrological loadings do interfere in the seismicity rates, by causing pressure stress changes and inducing earthquakes when the crust is close to its critical stress state.

3 GEOLOGICAL FRAMEWORK

3.1 AZORES ARCHIPELAGO

The Azores is an archipelago of volcanic origin located 1830 km from Portugal, at the junction of the American, Eurasian and African lithospheric plates, in the Middle Atlantic Ridge, North Atlantic Ocean. It is characterized as a shallow and triangular-shaped plateau. The plateau resulted from the intense volcanism that led to the formation of numerous seamounts and seven of the Azores islands (Luis and Neves, 2006).

The Azores archipelago is composed of nine volcanic islands: São Miguel and Santa Maria islands; Corvo and Flores islands; and Graciosa, Terceira, São Jorge, Faial and Pico islands. These islands are divided into three groups, the eastern, western (which lies in a stable tectonic environment), and the central group, respectively.

The archipelago has been often affected by large earthquakes followed by aftershocks, showing the typical mainshock/aftershock pattern (Silva et al. 2020).

Several hypotheses were proposed for the Azores plateau formation during the years, which involve tectonics and volcanism. Gente et al. 2003 suggested a hotspot located above a plume mantle as a driving mechanism for the formation of the plateau, which was developed before being tectonically rifted. Luis & Neves 2006 proposed that the elevation of the Azores plateau is mainly due to the thickened crust (Moho estimated at 12 km depth). The authors argued that the mantle upwelling triggered from above by extensional stresses and plate discontinuities lead to the accretion of large volumes of extrusives, accompanied by crustal growth in the form of underplating. Recent studies, such as Neves et al. 2013 demonstrated that the rifting of the upper brittle lithosphere of Azores may have occurred without the need of enhanced magmatic pulses related to mantle plume activity. Thus, although the development of the large volcanic systems that form the islands is a consequence of mantle processes, their emplacement and evolution are strongly constrained by tectonic processes, especially the lithospheric extension associated to the Terceira Rift (Neves et al. 2013).

The seismicity in the Azores is high but of low magnitude, and it is associated with volcanic activity and the triple junction geotectonic framework (Figure 4 and 5). It is concentrated along

the MAR and the Terceira Rift (TR), a succession of deep basins (reaching more than 3000 m deep) located at the northeast boundary of the eastern Azores plateau (Adam et al. 2013). The majority of the earthquakes have a shallow focal depth, less than 10 km. The majority of strongest earthquakes (M > 6) occur in the central group of islands, (Faial, Graciosa, Terceira, São Jorge e Pico), located directly on the Midge Atlantic Ridge (Silva et al. 2020; Gaspar et al. 2015).

Borges et al. 2007 state that the seismicity follows the same trend as the islands: approximately ENE from the Mid Atlantic Ridge to Terceira Island (where the 1980 and 1998 shocks were located) and SE from Terceira Island to São Miguel Island (Figure 4). The seismicity stops at 24°W, where the Terceira Ridge joins with the Gloria Fault, which is considered seismically inactive.

The focal mechanism of the Azores can be separated into two zones of distinct seismicity and stress direction. Zone I (from 30°W to 27°W) and Zone II (from 27°W to 23°W). Earthquakes located in Zone I (oriented ENE–WSW) show a predominant strike-slip motion with horizontal extension in N–S to NNE–SSW direction and horizontal E–W compression, whilst Zone II (oriented NW–SE), presents a horizontal extension in a NE–SW direction, normal to the Terceira Ridge (Borges et al. 2007).

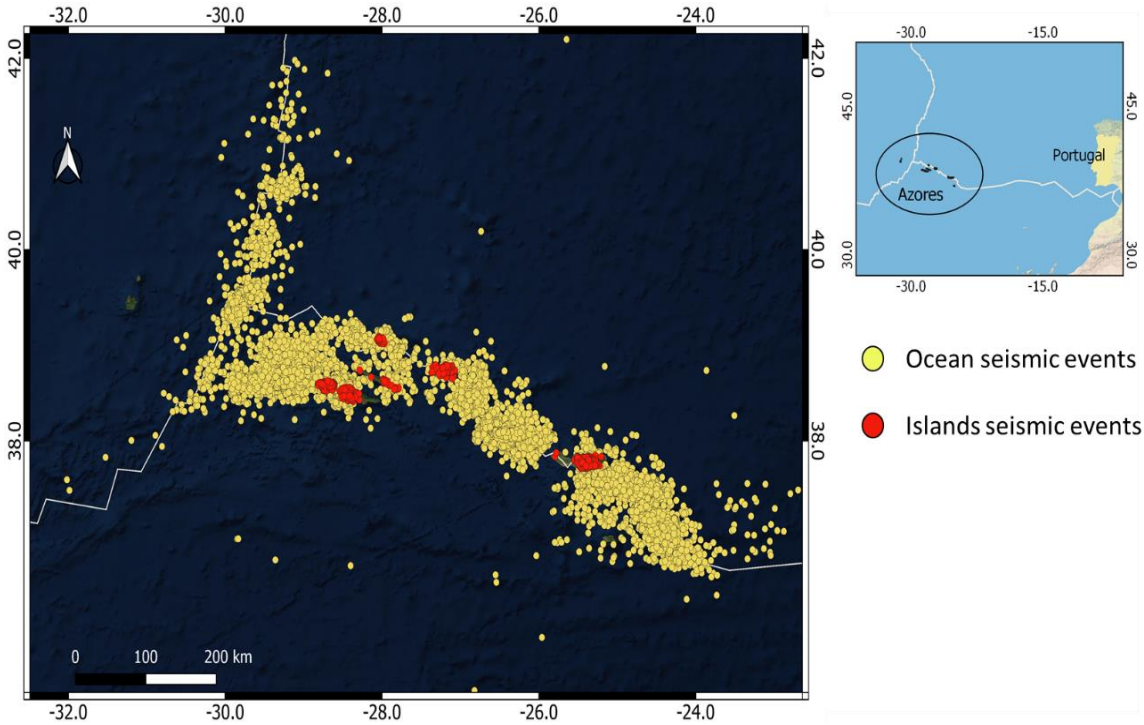

Figure 4. The Azores earthquake catalogue showing the seismicity in the region, from 2008 to 2018.

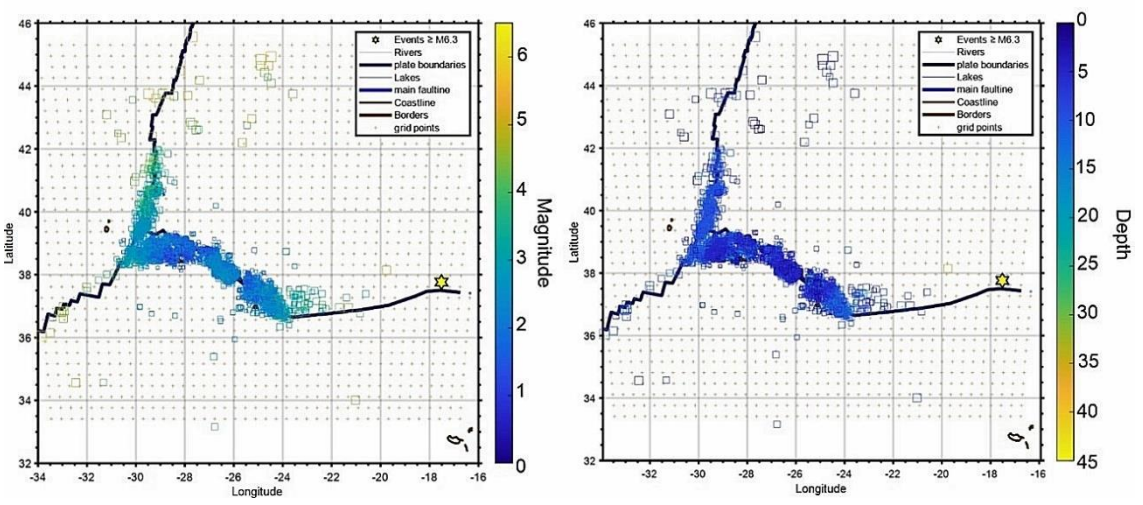

Figure 5. Earthquake catalogue of the Azores from 2008 to 2018 by magnitude (left) and depth (right).

In the last decades, the number of events recorded in the Azores increased due to the increasing number of operating seismic stations. According to Fontiela et al. 2018, nowadays earthquake clusters are detected at depths greater than 10 km, for instance beneath Graciosa Island, to the

east of Terceira, and beneath the central part of São Miguel island, in the region beneath Fogo-Furnas volcanoes.

4 METHODOLOGY

The methodology of this work is developed following the work of Craig et al. 2017 and Bollinger et al. 2007.

The methodology consists of three main steps, as shown by the flowchart (Figure 6):

(i) Manipulate seismic catalogues of the study areas and do the preprocessing of the data set, such as the declustering to eliminate seismic noises.

(ii) Apply statistical methods to test whether seasonality of the seismicity is genuine or not, following the Bollinger et al. 2007 approach.

(iii) Use decomposition methods, such as the Singular Spectrum Analysis (SSA) to investigate if the hydrological loading cycles coincide with seismicity cycles.

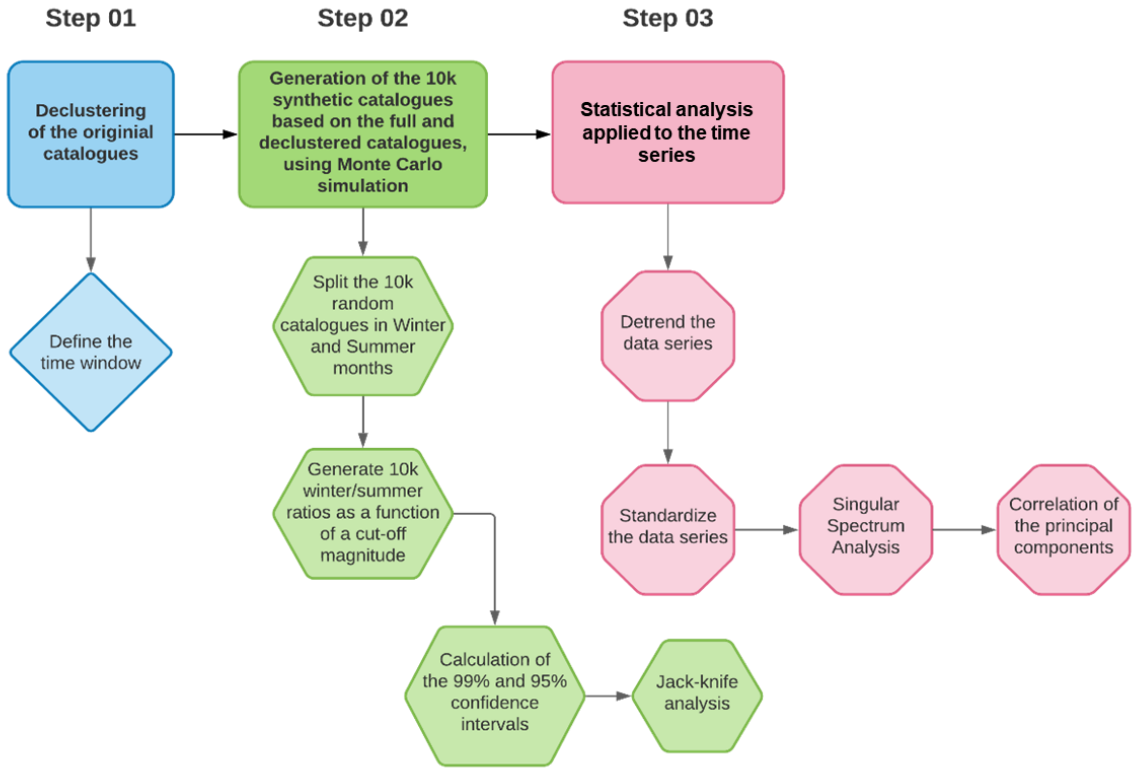

Figure 6. Flowchart of the processing steps of this work.

4.1 DATA SET

Earthquake catalogues are the primary source of information to study the seismotectonics and seismicity of an area. They contain the time and location of earthquakes, together with auxiliary information such as focal depth, estimated magnitudes and damage.

The seismic catalogue for the New Madrid region was obtained from the Center for Earthquake Research and Information (CERI), University of Memphis (Available at http://www.memphis.edu/ceri/seismic/catalog.php). The original catalogue dates from 1974 to the present day (Figure 7), but a time window from 2000 to 2015 was selected for the NMSZ following the Craig et al. 2017 approach, to maximize the uniformity of the catalogue and avoid biasing due to changes in the instrumentation.

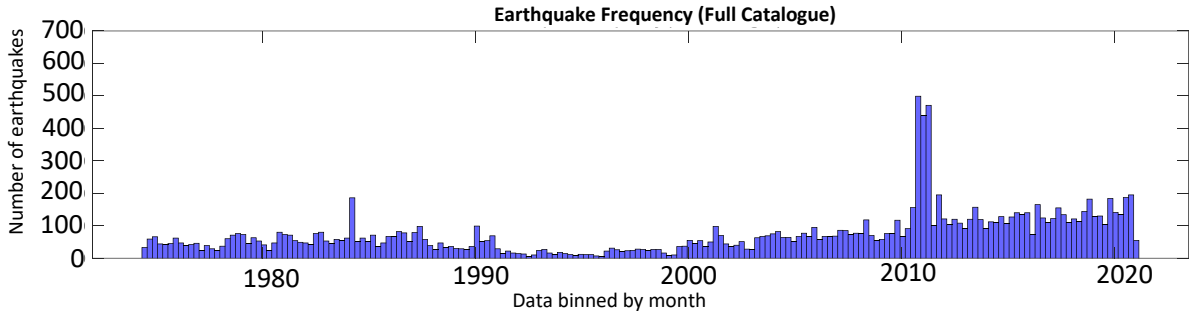

Figure 7. NMSZ catalogue from June 1974 to December 2020.

The Azores seismic catalogue was obtained from the Instituto Português do Mar e da Atmosfera (IPMA, Available at https://www.ipma.pt/pt/publicacoes/boletins.jsp?cmbDep=sis&cmbTema=bsi&idDep=sis&idTema=bsi&curAno=-1. The catalogue extends back to 1995 (Figure 8).

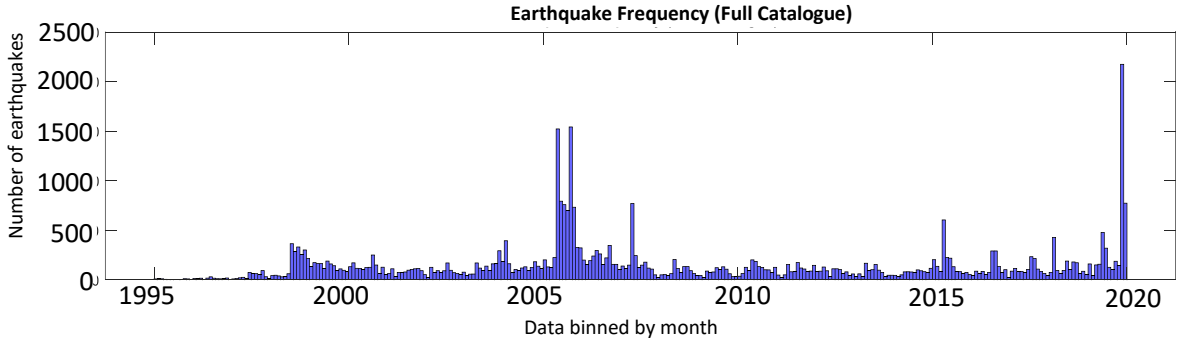

Figure 8. Azores catalogue from January 1995 to December 2019.

By visual inspection the Azores entire catalogue presents many peaks, mainly around 2007 and in 2019.

In November 2019 (the highest peak in Figure 8) indicates that more than 2.000 earthquakes were recorded during this month. According to Silva et al. 2020, more than 800 earthquakes were recorded in April 2007, which explains the peaks around this year. Moreover, in 2008 the Centre for Information and Seismovolcanic Surveillance of the Azores (CIVISA) was founded, and since then it manages the former seismic monitoring network. Thereby, to avoid biasing the results, the time window was limited from 2008 to 2018.

4.2 DECLUSTERING

The first step in the data processing is to decluster the original seismic catalogue following the Reasenbearg (1985) methodology, since the clustering of earthquakes masks weaker seismogenic processes.

According to Craig et al. 2017, large earthquakes produce thousands of aftershocks and foreshocks that introduce errors and reduce the statistical significance of seismicity. Therefore, to study the earthquake seasonality it is necessary to choose only independent earthquakes for an accurate evaluation of seasonal variations in seismicity. This process is called earthquake declustering and it helps to remove the aftershock/foreshock clusters that are dependent on the mainshock.

The declustering was applied on the Azores and NMSZ original catalogues and later limited to the desired time window. From 2008 to 2018 for Azores and from 2000 to 2015 for the NMSZ. The Azores catalogue was divided into island earthquakes and ocean earthquakes, since the physical processes that occur in both sites are different The islands suffer with local runoff, rivers load, sediment transport and rainfall, that can exert stress variations directly on the fault or may increase the pore fluid pressure at seismogenic depths, resulting in earthquakes. The ocean suffers with the pressure of the water column, tides and waves, as well as submarine landslides. Therefore, for a better analysis of the seasonality in both areas, the catalogue was divided.

The declustering process was done in ZMAP software (Wiemer 2001) that runs in MATLAB and follows the routines of Reasenberg 1985. ZMAP is a set of tools driven by a graphical user interface (GUI), designed to help seismologists analyze catalogue data (Wiemer 2001).

The data coming from catalogues is not homogeneous since the seismic waves are recorded by different instrumentation. The different networks employed, and their limitations introduce heterogeneities in the catalogues that vary in space and time and affect their quality. To avoid that, the quality of the earthquakes catalogues is assessed using a statistical parameter, the magnitude of completeness (Mc).

The Mc is the lowest magnitude for which all earthquakes in space and time are reliably recorded, and it may vary in space and time. To estimate the magnitude of completeness, the maximum of the derivative of the frequency magnitude distribution is used.

The frequency magnitude distribution of the catalogues (Figure 9a, b) is described by the relationship between the frequency of occurrence and the magnitude of the earthquakes, which is known as the Gutenberg-Richter power law (Gutenberg & Richter 1944):

$$log_{10} N(M) = a - bM \quad (1)$$

Where N is the number of earthquakes having a magnitude larger than M, a and b are constants. The a-value describes the total seismicity rate of the region, while the b-value relates to tectonic stress. It is common in volcanic areas to have high b-values, up to 2, due to the high-temperature gradient or due to the presence of a buoyant mantle upwelling (Warren & Latham 1970; Adam et al. 2013), while b-values lower than 1 indicate zones of high applied shear stress or increase in effective stress (Scholz 1968; Wyss 1973 fide Fontiela et al. 2014). The b-value is automatically estimated considering the magnitude of completeness.

The Gutenberg-Richter Law groups earthquakes into "bins" based on the number of events with magnitudes larger than each reference magnitude (Figure 9c, d). For example, an M3 bin would include all events greater than or equal to 3. The count in each bin is then plotted on a common logarithmic scale. If this were a statistically perfect dataset, the data would form a straight line from the lowest magnitude to the highest. When a straight line is fit to the data, the point where our data separates from the line is our magnitude of completeness (Gardine 2020, Alaska

Earthquake Center). An earthquake catalogue with lower Mc captures the whole seismic picture better. Moreover, in the context of a regional network, the Mc demonstrates where the monitoring capabilities are strongest and what areas might be lacking.

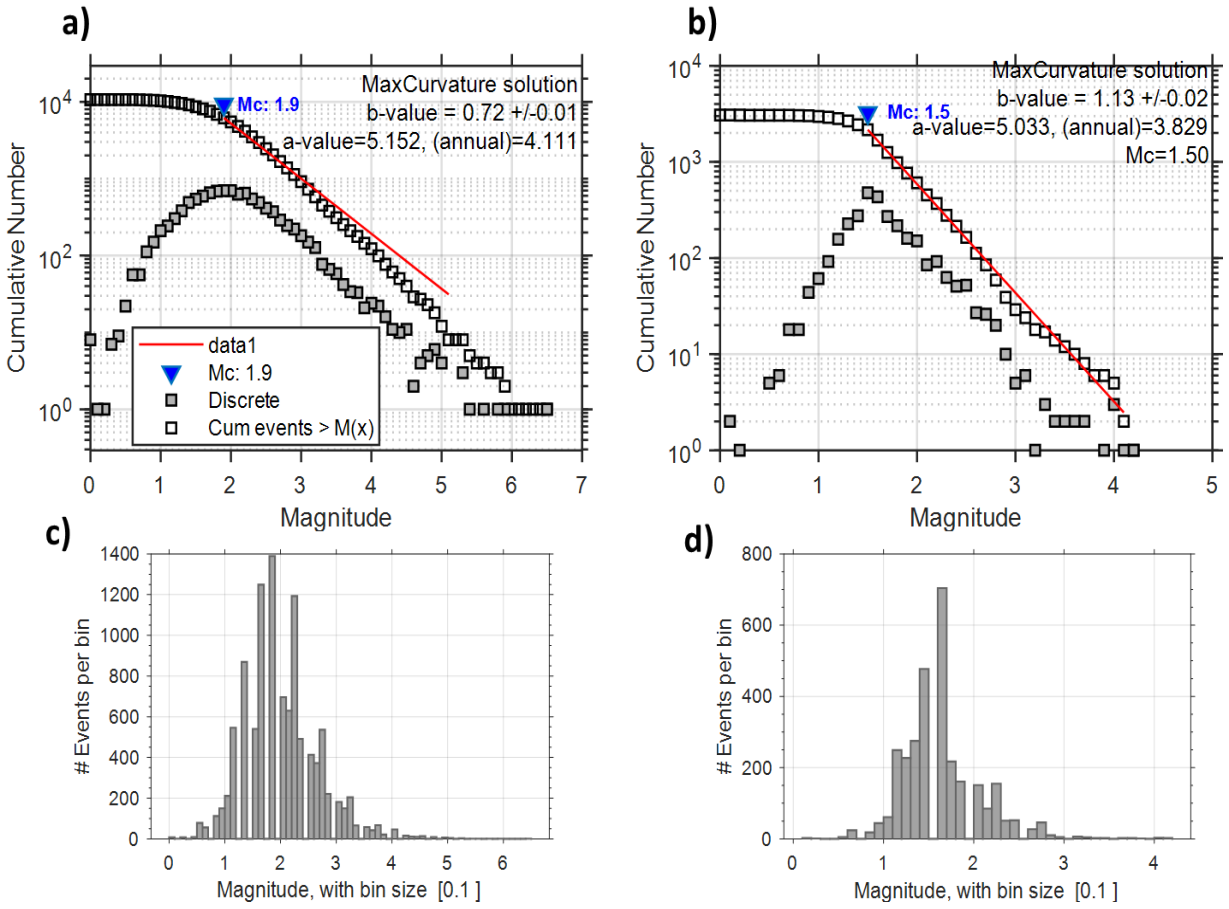

Figure 9. Frequency magnitude distribution of the **(a)** Azores and **(b)** NMSZ declustered catalogues, the magnitude of completeness as determined by the derivative (blue triangle) and the a, b-values. **(c)** Magnitude grouped per bins for Azores and **(d)** NMSZ.

The filled squares in Figure 9 represent the derivative of the frequency magnitude distribution, used to define the Mc. The red line is the Gutenberg-Richter power law fitted for the declustered data, which begins at the minimum magnitude of completeness (the highest point of the derivative curve).

4.3 MONTE CARLO SIMULATION

The statistical methods applied in this work follow the Bollinger et al. 2007 approach, and test if the seasonality of the seismicity is genuine.

The approach consists of running a Monte Carlo simulation to generate 10.000 random seismic catalogues based on the full and declustered data. Bollinger et al. 2007 proposed that the random catalogues should have the same number of events and frequency magnitude distribution as the real catalogues, in order to test the statistical significance of the data.

The Monte Carlo method relies on massive random sampling to obtain numerical results, which means, repeating successive simulations many times using probability functions to estimate the possible outcomes of an uncertain event. During the simulation, a random value is assigned to the variable that has uncertainty. The model is then run, and a result is provided. This process is repeated *N* times while assigning the variable in question with many different values. Once the simulation is complete, the results are averaged together to provide an estimate. The method is used to understand the impact of risk and uncertainty in prediction, as well as forecasting models.

The ZMAP software allows the generation of one single random catalogue, therefore a MATLAB routine was created based on the original software to run the 10.000 random simulations, considering the real catalogues (Figure 10).

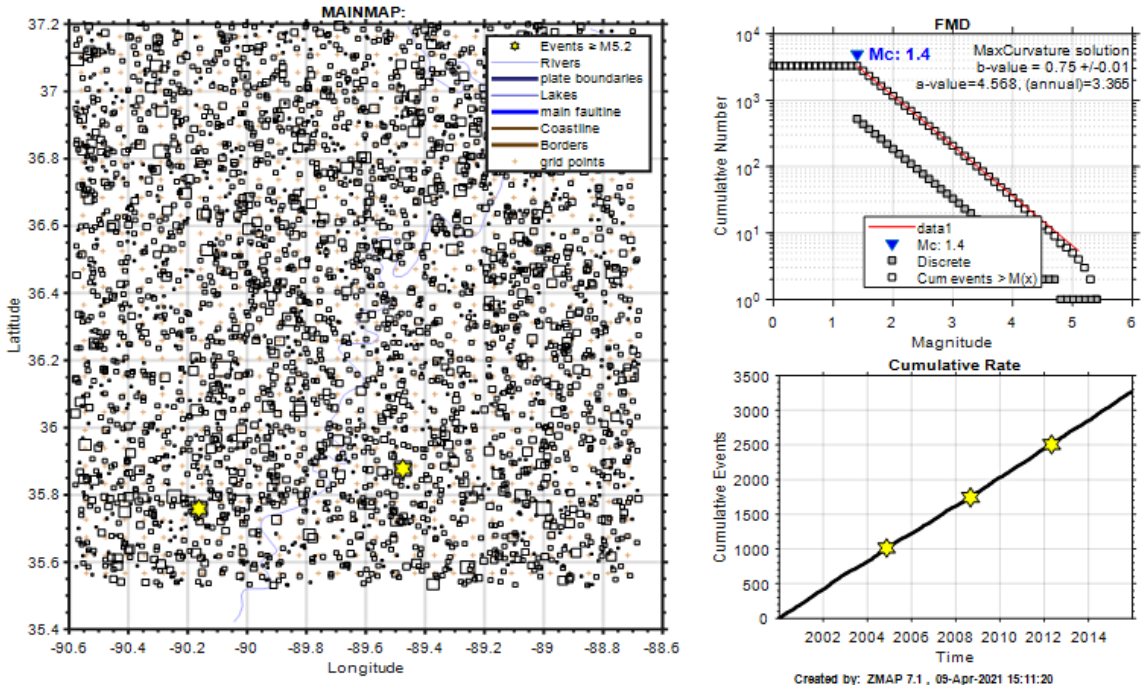

Figure 10. An example of one random catalogue generated by Monte Carlo simulation based on the New Madrid Seismic Zone full catalogue.

First, the simulation was ran based on the full catalogues of Azores and New Madrid Seismic Zone, one at a time, and later it was repeated for the declustered catalogues. Prior to the simulation, it is necessary to introduce the parameters of the original catalogues, such as the number of events, b-value, magnitude of completeness, maximum and minimum longitude and latitude, maximum and minimum depth, etc., so during the process, random values are assigned to these parameters.

Further, each one of the 10.000 random catalogues was split into Winter (January to Abril) and Summer (July to October) months and their ratios were calculated as a function of a cut-off magnitude, as shown in Figure 11, following the Bollinger et al. 2007 methodology. At last, the 99% and 95% confidence limits were calculated to test the real ratio observation against the simulation.

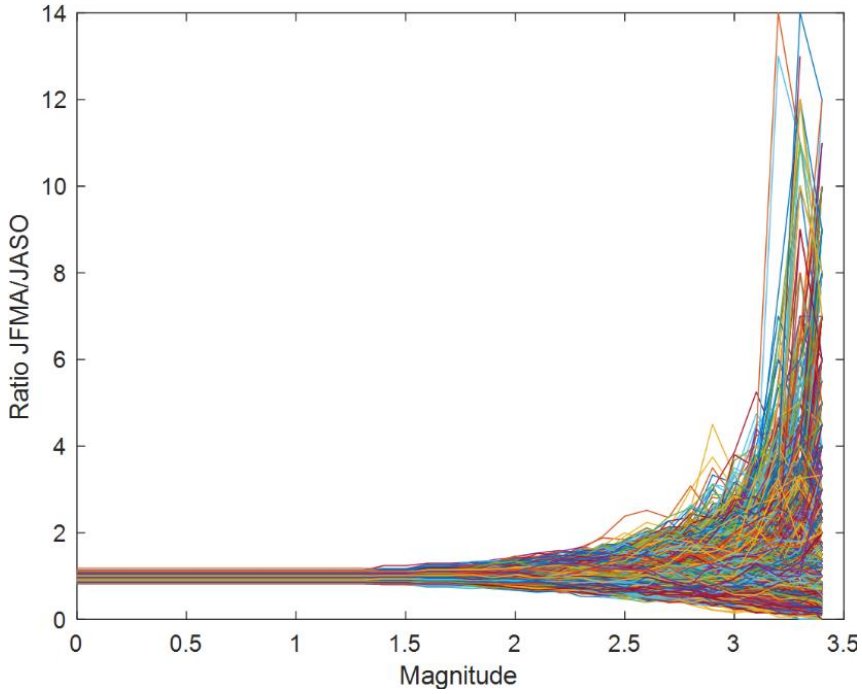

Figure 11. 10.000 ratios Winter(JFMA)/Summer(JASO) coming from the 10.000 random catalogues, generated by Monte Carlo simulation based on the New Madrid Seismic Zone full catalogue.

Figure 12 shows the approach aforementioned, applied by Bollinger et al. 2007 in Nepal.

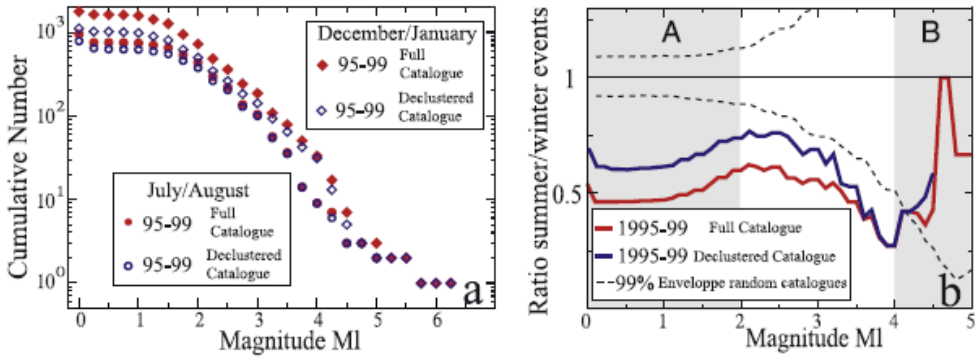

Figure 12. **(a)** Frequency magnitude distribution for winter months (diamonds) and summer months (circles). The open symbols indicate the declustered catalogue. **(b)** A test for the possibility of observing the summer/winter variation by chance, compared to the observed ratio (blue and red solid lines) for different magnitudes. The dashed curves are the summer/winter ratios that contain 99% of the summer/winter ratios derived from the 10.000 random catalogues, with the same frequency magnitude distribution as the real catalogue. (from Bollinger et al. 2007).

The authors concluded that the probability that the observed low ratio of summer/winter events would be due to chance is much less than 1% up to magnitude 4, as well as lower than the 99% envelope of the 10.000 random catalogues (dashed lines). It was concluded that instrumental effects are not able to produce an artificial seasonality at such high magnitudes, hence the seasonality of the study area, in which the seismicity is enhanced during Winter when compared to Summer, is genuine.

4.4 JACK-KNIFE ANALYSIS

The Jack-Knife analysis is employed following the work of Craig et al. 2017, with the purpose of identifying if the seasonality may be occurring due to extreme events in one of the years.

The Jack-Knife is determined generating the 10.000 ratios, as mentioned in the previous section, but now removing one calendar year of data from the original seismic catalogue, in each test. Further, the residuals of the analysis are determined by the difference of the observed ratio and the 95% confidence interval for each test.

4.5 SINGULAR SPECTRUM ANALYSIS (SSA)

The relation between hydrological loads and earthquakes is addressed using high-quality time series of monthly seismicity rate, rainfall, atmospheric and sea level pressure, and monthly significant height of combined wind waves and swell.

The Singular Spectrum Analysis (SSA) employed to identify modes of oscillation in order to recognize common patterns in seismicity and water loads, as presented in Figure 3.

The SSA is a form of principal component analysis that allows analyzing spatial and temporal correlations between different time series to extract empirical orthogonal basis functions that represent their common modes of spatiotemporal variability (Craig et al. 2017; Gruszczynska et al. 2018).

The SSA analysis is done only for the Azores region, using the HydroClimATe software, developed by the Arizona Water Science Center and California Water Science Center (Dickinson et al. 2014) and implements the approach proposed by Broomhead & King (1986). It consists of two stages: decomposition of the grand-covariance matrix and reconstruction of the interesting component (Gruszczynska et al. 2018).

The approach of Broomhead & King 1986, utilizes a trajectory matrix *X* that is composed of a series of windows of the time series that are of length *M*. The dimensions of *X* are M_T by N_T (Dickinson et al. 2014).

Where,

N_T is equal to $M - N + 1$;

N is the number of time steps in the time series;

M_T is the embedding dimension of X.

The forwarded step is the calculation of the covariance matrix, given by the following equation:

$$C = \frac{DD^T}{N_T} \tag{2}$$

Where,

C is an M_T by M_T covariance matrix;

D is an M_T by N_T trajectory matrix;

D_T is the transpose of X.

The eigenvectors and eigenvalues of C are obtained by an eigenanalysis of C:

$$CE = \lambda E \tag{3}$$

Where,

E is an M_T by M_T matrix of the eigenvectors, and λ is the vector of eigenvalues of length M_T.

The matrix of the principal components A, is obtained by projecting the eigenvectors *E* onto the trajectory matrix *D*, and finally the reconstructed components (RCs) are formed by convolution of the principal components with the eigenvectors, as described by Ghil et al. 2002:

$$R_K = \frac{1}{M_T} \sum_{k \in K} \sum_{j=L_T}^{U_T} A_k(t-1+1)\, E_k(j) \quad (4)$$

Where,

K is the set of eigenvectors that are used in the reconstruction,

M_T is a normalization factor;

L_T is a bound of summation;

U_T is a bound of summation.

The monthly rainfall, atmospheric and mean sea level pressure, and the significant height of combined wind waves and swell time series, used in the SSA analysis were obtained from the ERA5 dataset developed by the ECMWF (European Centre for Medium-Range Weather Forecasts) that covers the Earth on a 30km grid (available at https://www.ecmwf.int/en/forecasts/datasets). The monthly seismicity rate was calculated from the declustered ocean Azores catalogue described in section 4.2.

Each one of the time series was detrended and standardized to a normal distribution, for comparisons across data types, prior to the SSA analysis (Figure 13 a-j).

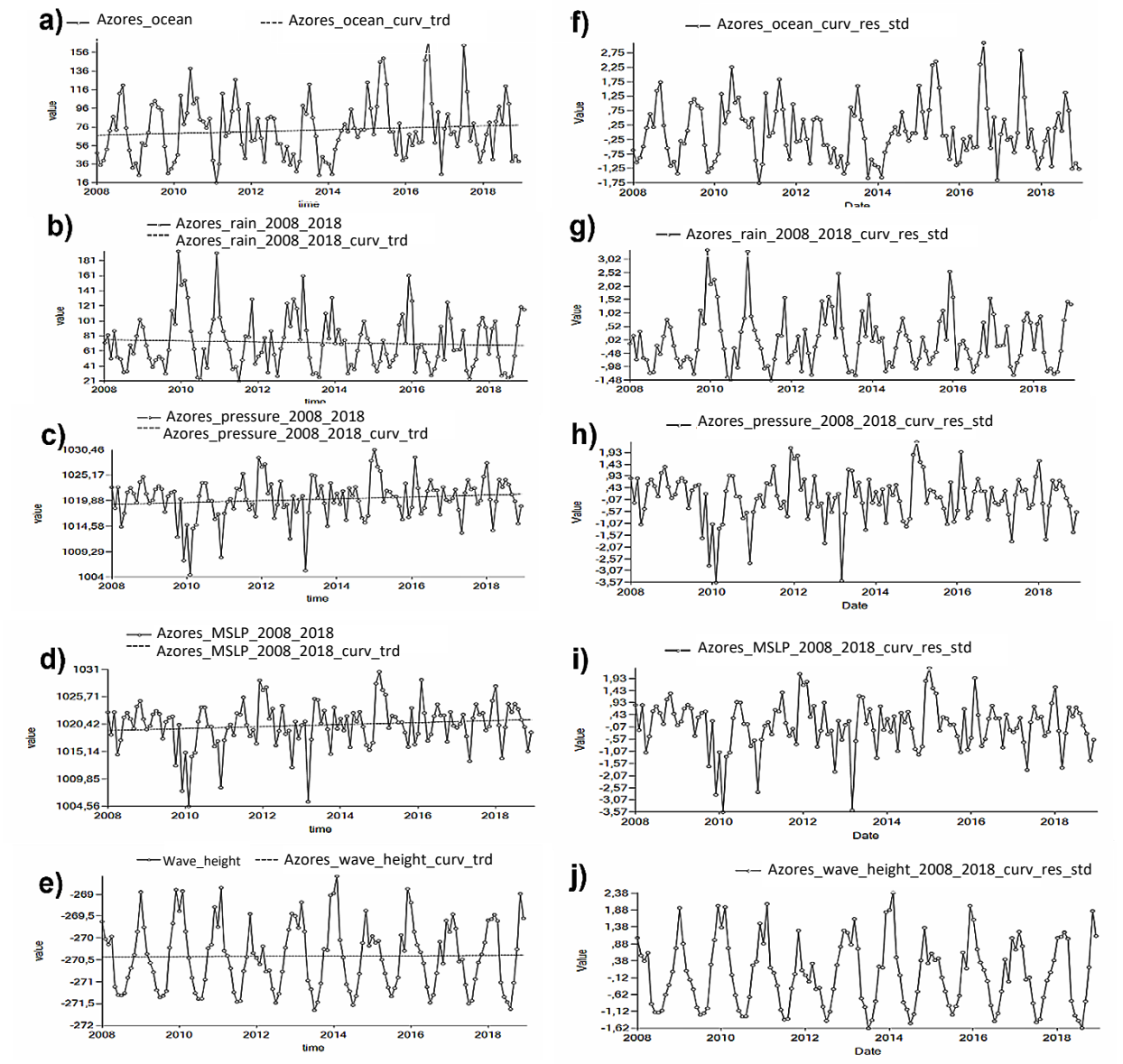

Figure 13. Detrend of the **(a)** Azores monthly seismicity rate, **(b)** monthly rainfall, **(c)** monthly atmospheric pressure, **(d)** mean sea level pressure, **(e)** significant wave height, **f-j** show the standardization of correspondent time series residuals.

During the analysis, the window length, and the method of calculating the error bars of spectral estimates were defined. The window length needs to be wide enough to contain sufficient data over the oscillatory component and it was set at 13. By default, the program sets the window length to be one-tenth of the total number of points (in this case, 132 points). The error bars, which is an *ad hoc* significant test help to assess the significance of the components by visual

inspection of the spectrum and the error bars, and it was calculated using the Vautard & Ghil method (Vautard & Ghil 1989), as shown in Figure 14.

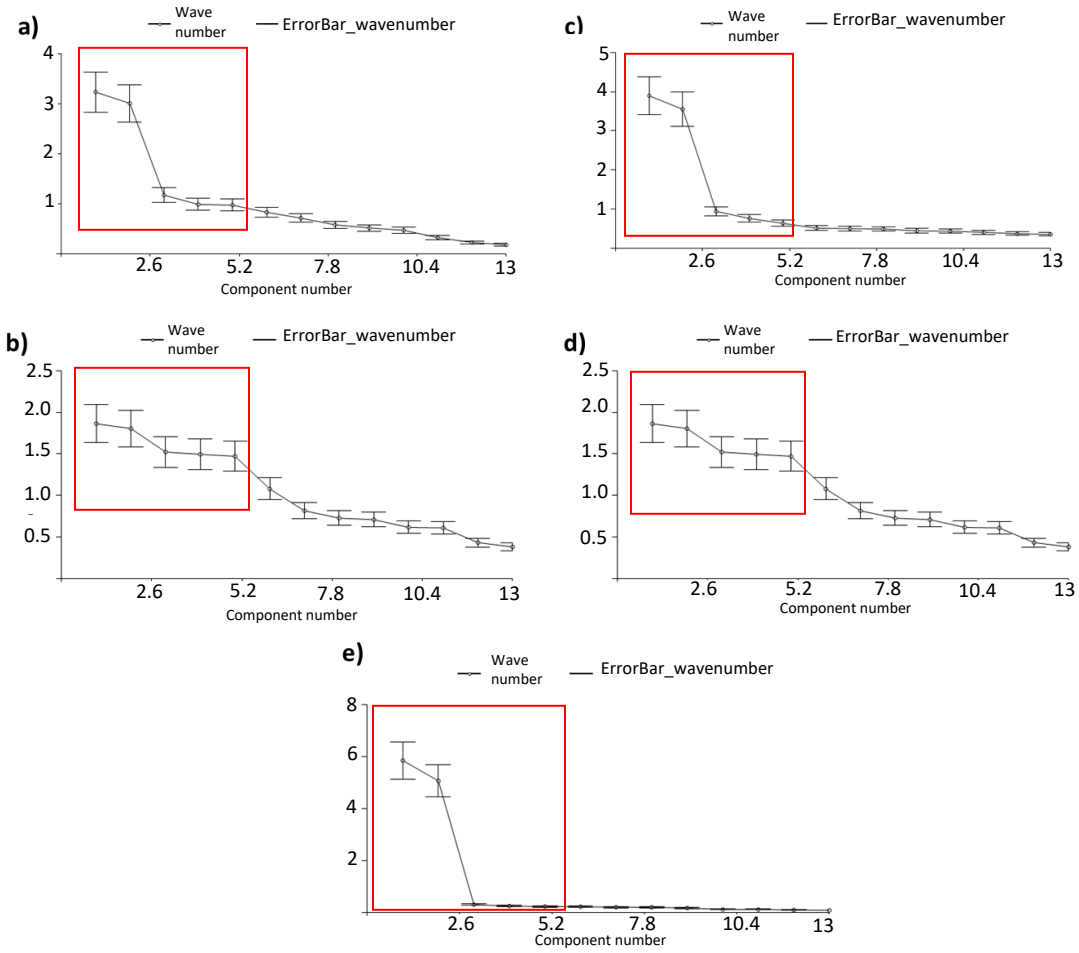

Figure 14. Error bars of spectral estimates for the **(a)** Azores ocean seismicity rate, **(b)** atmospheric pressure, **(c)** rainfall, **(d)** mean sea level pressure, and **(e)** significant height of combined wind waves and swell. The five first components (red boxes) were selected to the correlation according to their percent variance. The five first components contribute: 74 % to the signal of the ocean seismicity rate, 60% to the atmospheric and mean sea level pressure, 71% to the rainfall and 84% to the significant wave height.

Significant components (such as the first two annual components in Figure 14a) contribute more variance than that from noise background and tend to be separated from the components on the flatter, right side of the spectrum by the length of the error bars (Dickinson et al. 2014).

Lastly, the five first reconstructed components (RCs) of each time series were chosen to be correlated with the RCs of the ocean seismicity rate.

4.6 LINEAR REGRESSION AND CORRELATION ANALYSIS

Linear regression and the evaluation of the Correlation between data series are useful tools for exploring linear relations and for investigating the phase shift of the dependent time series.

The Linear regression, as well as the Correlation analysis was done using the sum of the reconstructed components of the ocean seismicity rate, rainfall, atmospheric and mean sea level pressure, and significant wave height time series. The process was done in the HydroClimATe software, in which it was used a two-tailed significance test at a 95% confidence level to evaluate the significance of the correlation coefficient.

5 NEW MADRID SEISMIC ZONE – THE BENCHMARK

The New Madrid Seismic Zone (USA) is an active intraplate fault system located in the central area of the North American Plate. The fault system is considered a right-lateral strike-slip fault with about 70 km wide and 200 km long, formed when North America began rifting apart (Figure 15).

The fault system lies on the northern part of the Mississippi embayment and it is cut by the river. According to Craig et al. 2017, the northern flank of the Mississippi is a site of major annually varying hydrological load, which interferes in the seismicity, since the reduced water load in late summer and autumn promotes failure of the active fault system.

The NMSZ study area was defined in QGIS software (QGIS.org, 2021), where it was applied a mask to limit the seismicity inside the yellow polygon (Figure 15), which was the same area used by Craig et al. 2017.

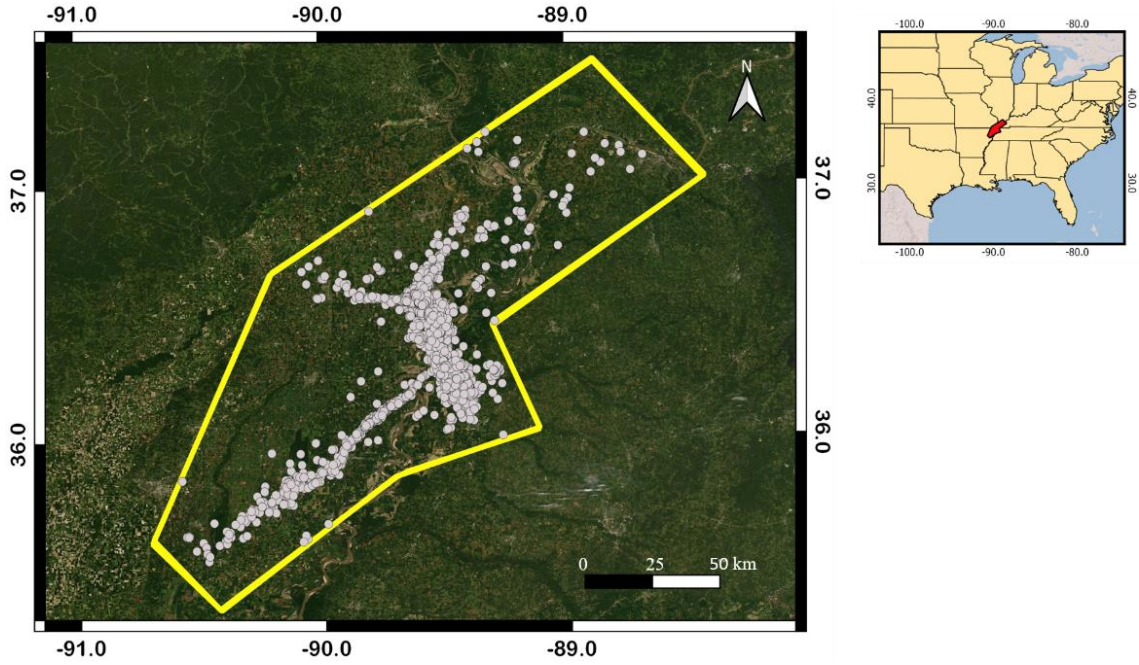

Figure 15. Seismicity on the New Madrid Seismic Zone (yellow polygon) from the full earthquake catalogue, from 2000 to 2015 and its location in the United States (red polygon).

The earthquake activity in the New Madrid region is spatially associated with the Reelfoot rift (Figure 16), which is covered by up to 6 km of Phanerozoic sediments formed during the

breakup of the supercontinent Rodinia (USGS; Csontos & Arsdale 2008). The Reelfoot Rift is identified as a reverse fault system that extends northwest from near Dyersburg, Tennessee, to New Madrid, Missouri.

The New Madrid seismicity may be produced by movement on old faults in response to compressive stress related to plate motions (USGS). The earthquakes hypocenters lie almost exclusively between 3 km to 15 km depth range (Figure 17) and are driven by ongoing strain accrual processes that despite low deformation rates are not decaying with time. (Pratt 1994; Page & Hough 2014).

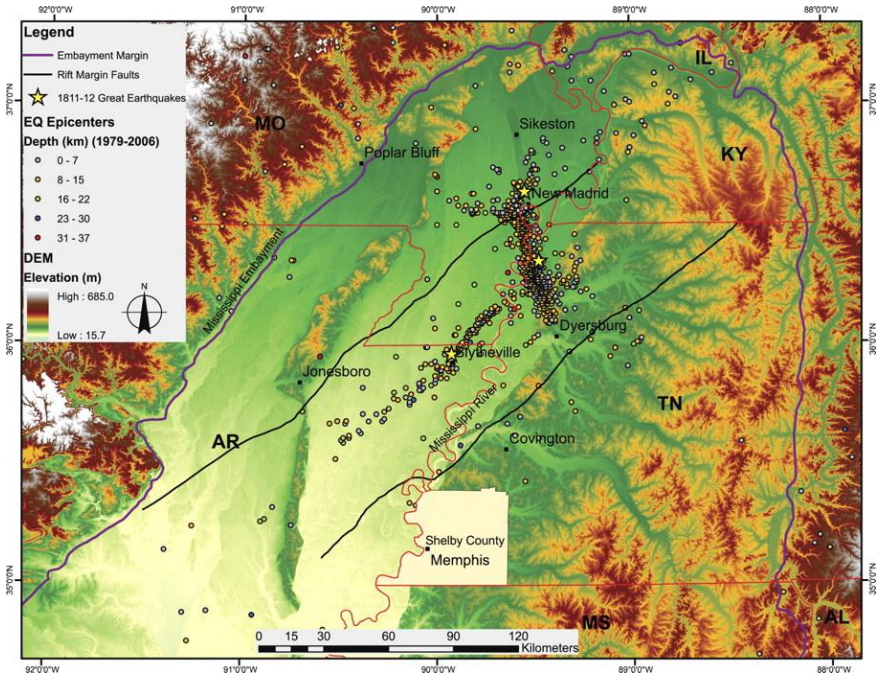

Figure 16. Reelfoot rift bounded by black lines and Mississippi embayment bounded by the purple line. Microearthquake activity as colored stars at estimated locations of the 16 December 1811 (south), 23 January 1812 (north), and 7 February 1812 (central) earthquakes. (from Csontos & Arsdale 2008).

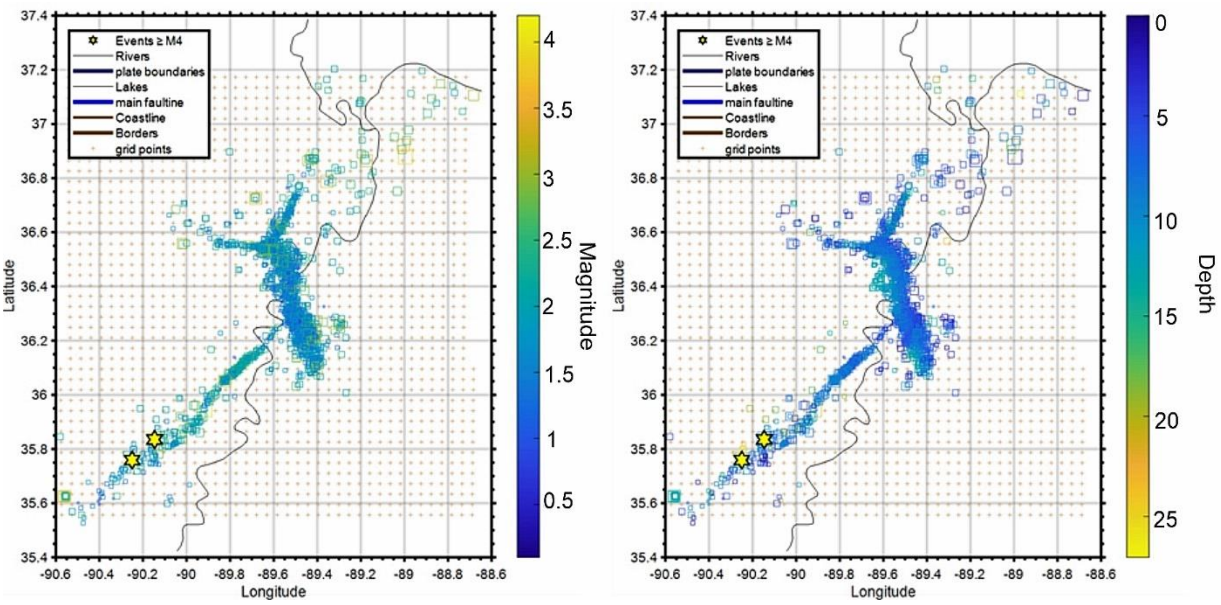

Figure 17. Earthquake catalogue of the NMSZ from 2000 to 2015 by magnitude (left) and depth (right). The black line cutting the fault system represents the Mississippi River.

Craig et al. 2017 point out the NMSZ region experienced a pulse of four major (M > 7) earthquakes in 1811–1812 and has been presenting low-level seismic activity ever since, rarely exceeding M3 (Figure 17). Despite its low magnitude earthquakes, the NMSZ is one of the most hazardous earthquake zones in the United States, due to its liquefaction susceptibility that makes the soil loses stiffness due to tectonic stresses.

5.1 Seasonal Variations in the New Madrid Seismic Zone Seismicity

Following Craig et al. 2017 approach, the NMSZ original catalogue (dated from 1974 to 2020) is limited from 3 January 2000 to 30 December 2015, containing 3.274 events, summarized in Figure 15.

The declustering of the catalogue applied prior to the time window selection helped to remove sharp jumps in the cumulative number of earthquakes, coming from aftershocks. The

declustering process found 537 clusters in the original catalogue, which corresponds to 2.480 events of 13.987 events.

Assuming a Gutenberg Richter magnitude frequency distribution, the full and declustered NMSZ catalogue is complete down to and including M1.5 (the magnitude of completeness), shown in Figure 18. For comparison purposes it was used M1.4 in the further calculations, the magnitude of completeness obtained by Craig et al. 2017.

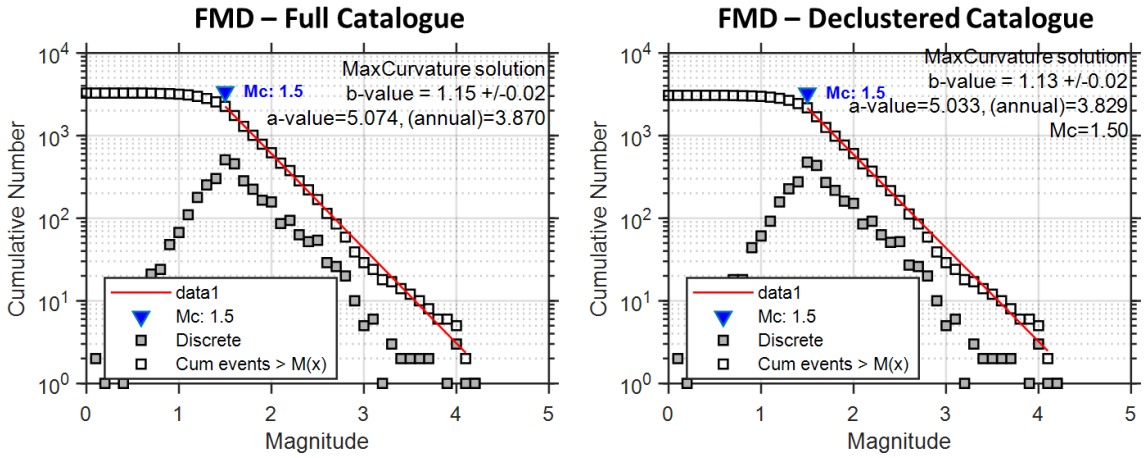

Figure 18. Frequency magnitude distribution (FMD) for the full and declustered New Madrid Seismic Zone catalogue.

The earthquake frequency for the full and declustered catalogues (blue bars) and considering only the earthquakes above the magnitude of completeness 1.4 (red bars) are plotted in Figure 19a and Figure 19b to observe if seasonal patterns are present. Rapid pulses in seismic activity are visible in the detrended cumulative rates plot, shown in Figure 19c. Peaks around 2008 were successfully removed on the declustering.

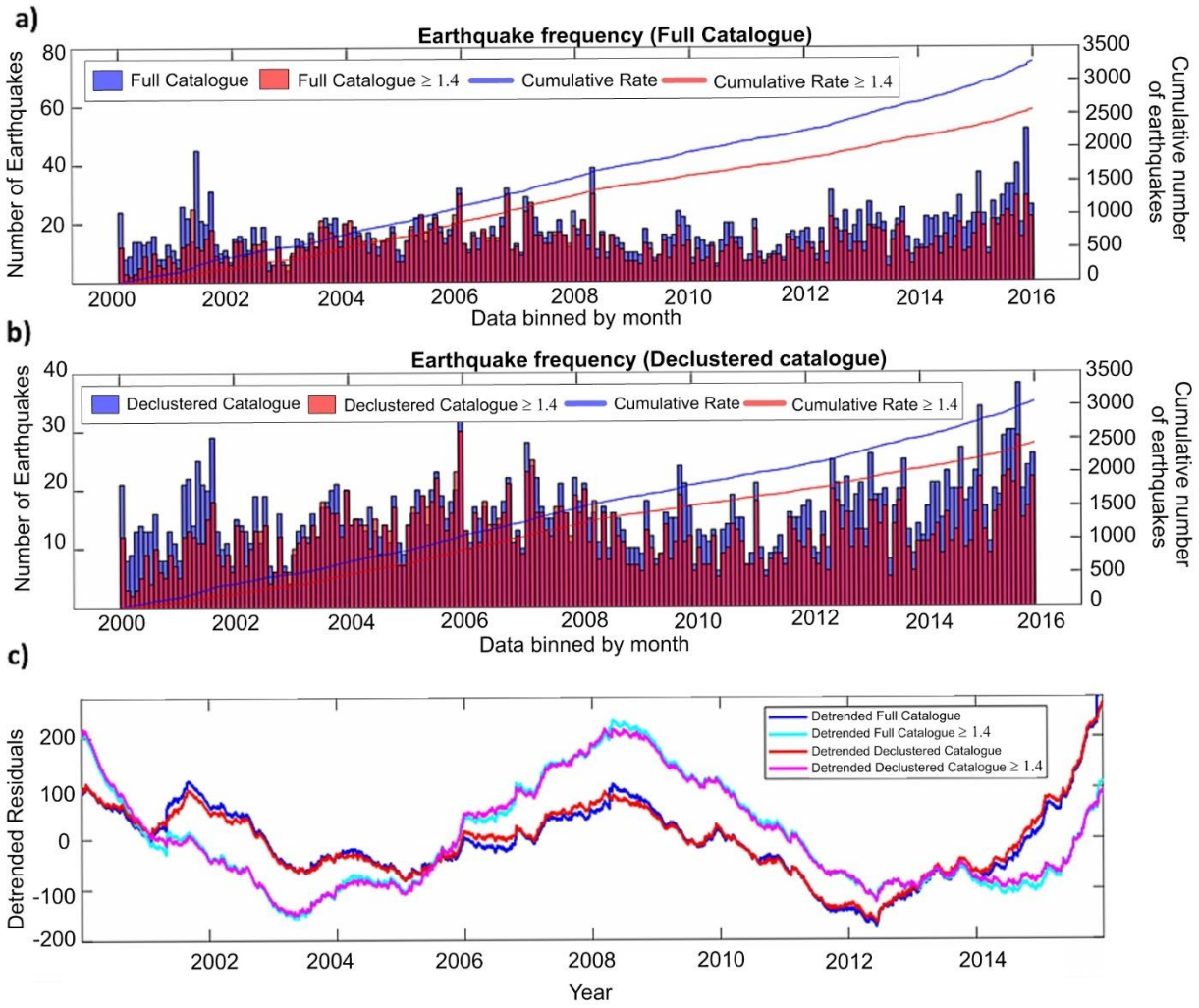

Figure 19. **(a)** Histogram frequency distribution for the full NMSZ catalogue (blue) and considering only earthquakes >= M1.4, and their respective cumulative rates. **(b)** is like **(a)** but for the declustered catalogue. **(c)** Cumulative number of earthquakes with a best-fit linear trend removed. Detrended residuals for the full catalogue (Dark blue), detrended full catalogue M >= 1.4 (Light blue), detrended declustered catalogue (Red), and detrended declustered catalogue M >= 1.4 (Magenta).

Figure 20a, 20d presents the variability of the original and declustered catalogues stacked on an annual timescale divided into 2-month bins. The histograms show a tendency for seismicity in late summer/early autumn (July-August-September-October) and a low tendency in spring (January-February-March-April), as observed by Craig et al. 2017. Taking the synthetic data set consisting of 10.000 random seismic catalogues and calculating the 95% and 99% confidence

limits for observing a ratio between events in JFMA months to JASO months that is significantly lower than 1, the observed seasonality was proved to be genuine.

Considering the full and declustered catalogues (Figure 20b, e) the probability that the observed low ratio would be due to chance is less than 1% for specific magnitude bands from M1.4 (the magnitude of completeness) to M2.1 and from M1.4 to M2.2, considering the 99% and 95% confidence limits, respectively. At higher magnitude bands the number of earthquakes is insufficient to provide a statistically significant trend.

The ratio exceeds the confidence limits most at M>1.9, where the variation results in approximately 60% more events in JASO than in JFMA (Craig et al. 2017).

Figure 20c and Figure 20f present the residuals of the Jack-Knife analysis, calculated to test if the seasonality is being influenced by extreme climatic events or deviations that might have been caused by the declustering. The residuals show that by removing one calendar year of data from the seismic catalogue, the seasonality is not a result of a single extreme event. The results of the Jack-Knife analysis removing each one of the years from the data set (from 2000 to 2015) are found in appendix A.

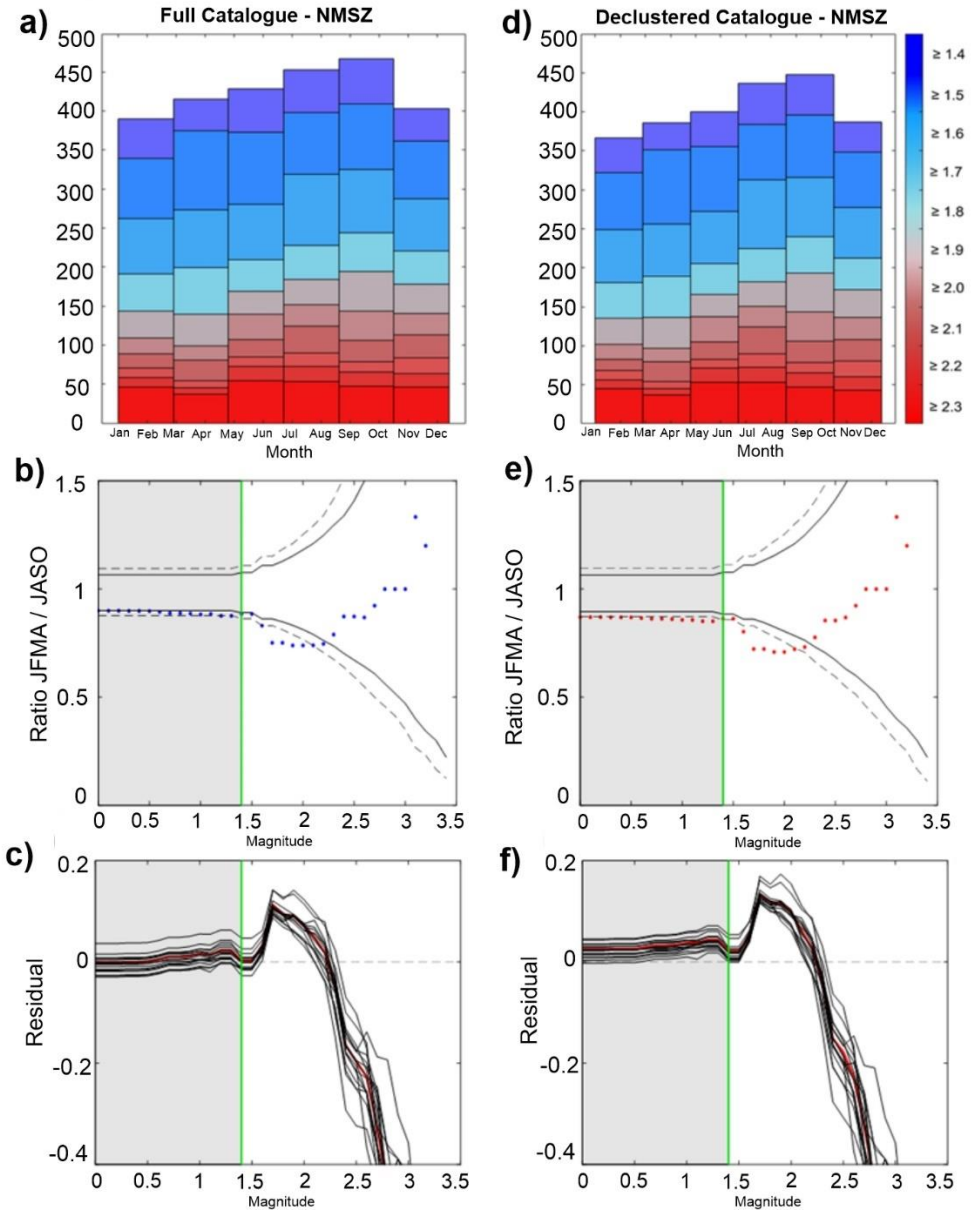

Figure 20. **(a)** Histogram for the seismicity of the NMSZ stacked on an annual timescale (divided into 2-month bins) between 1 January 2000 and 31 December 2015. Colors on the histogram indicate the magnitude cut-off used in each case. **(b)** Observed ratio (blue dots) of the number of earthquakes occurring in January, February, March, April, to those occurring in July, August, September, October as a function of cut-off magnitude. Grey shaded areas indicate the magnitude of completeness 1.4. Dashed and solid black lines indicate the 99% and 95% confidence limits, respectively. **(c)** Residuals of the Jack-knife analysis. The black lines indicate the residual at each magnitude band between the calculated ratio and the 95% confidence limit. The ratios are calculated for the same catalogue but removing each

calendar year of the data. The red line represents the residuals of the observed ratio (the blue dots shown in **c, d)**. The confidence limits are estimated independently for each test. Positive values are those where the magnitude bands exceed the confidence limits in **b**. **d–f** are as **a–c**, but for the declustered seismic catalogue.

The results found for the New Madrid Seismic Zone are similar to the results obtained by Craig et al. 2017 where the seismicity is enhanced during the summer, confirming that the applied methodology is reliable to be applied in the Azores region. For comparison purposes, the results obtained by the author are available in Annex A.

6 RESULTS

The original Azores catalogue (dated from 1995 to 2019) was limited in time to maximize the uniformity of the catalogue and to avoid biasing the results due to changes in the instrumentation. The time window was set from 1 January 2008 to 31 December 2018, containing 13.492 events.

The sharp jumps in the cumulative number of earthquakes, coming from aftershocks were successfully removed from the catalogue by the declustering process. The declustering was applied to the original catalogue, from 1995 to 2019 (41.539 seismic events), prior to the temporal window selection, and found 2.735 clusters which correspond to 18.673 events of 41.539 events.

The seismicity in the Azores includes earthquakes in the islands and in the ocean. To better analyze the seasonal trends, the catalogue from 2008 to 2018 was divided in islands and ocean earthquakes and analyzed separately, as explained in section 4.2

Considering the Gutenberg Richter magnitude frequency distribution, the full and declustered catalogues for the islands present 1.773 and 1.118 events, respectively, and are complete down to and including M1.4, the magnitude of completeness (Figure 21a, b). In the oceans the number of events is much larger. The full and declustered catalogues of the ocean have 11.719 and 9.572 events, respectively, and are complete down to and including M2.0, the magnitude of completeness (Figure 21c, d).

The complete data set (islands and ocean seismic events) presents a M1.9 magnitude of completeness (Figure 9a) and is mostly explained by the ocean catalogue.

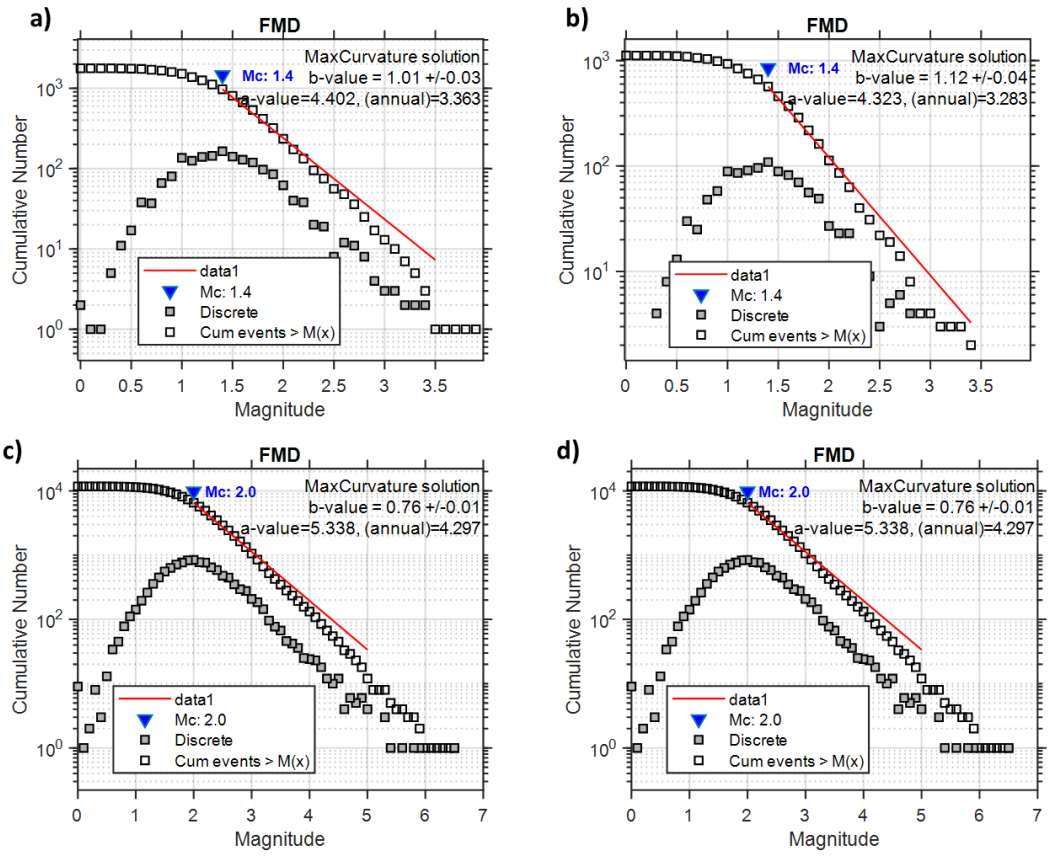

Figure 21. Frequency magnitude distribution (FMD) for the **(a)** full and **(b)** declustered Azores islands catalogue, and **(c)** full and **(d)** declustered Azores ocean catalogue.

The magnitude of completeness is higher in the catalogue of the ocean because there is a chance of earthquakes lower than M2.0 not being recorded due to the oceanic background noise, which is the residual sound when known sources of sound are removed. These frequencies capture by the seismic sensors are generated by natural sources such as rainfall, turbulence, waves and tides, or by anthropogenic sources like vessels, and hinder the recorded of small magnitude earthquakes.

6.1 SEASONAL VARIATIONS IN THE AZORES ISLANDS SEISMICITY

To observe if seasonal patterns are present, the earthquake frequency of the islands for the full and declustered catalogues (blue bars) and considering only the earthquakes above the

magnitude of completeness M1.4 (red bars) are plotted in Figure 22a and Figure 22b. The rapid pulses in seismic activity are visible in the detrended cumulative rates plot (Figure 22c). Peaks around 2018, were successfully removed on the declustering process that smoothed the seismicity rate. To confirm if the catalogues present seasonality the data was stacked on an annual timescale and divided into 2-month bins, as shown in Figure 23a, d.

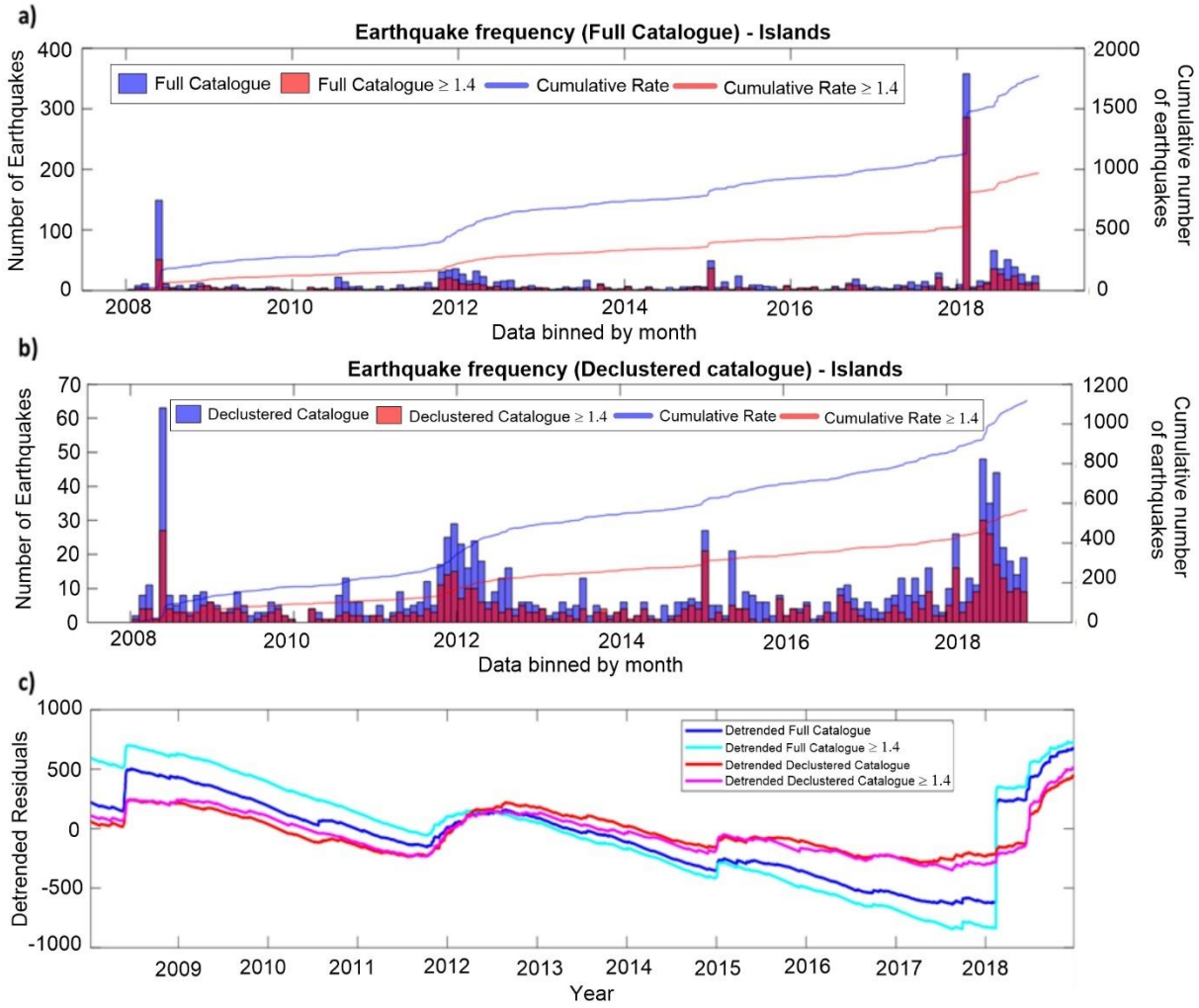

Figure 22. **(a)** Histogram frequency distribution for the full Azores islands catalogue (Blue) and considering only earthquakes >= M1.4 (Red), and their respective cumulative rates. **(b)** is like **(a)** but for the declustered catalogue. **(c)** Cumulative number of earthquakes with a best-fit linear trend removed. Detrended residuals for the full catalogue (Dark blue), detrended full catalogue M >= 1.4 (Light blue), detrended declustered catalogue (Red), detrended declustered catalogue M >= 1.4 (Magenta).

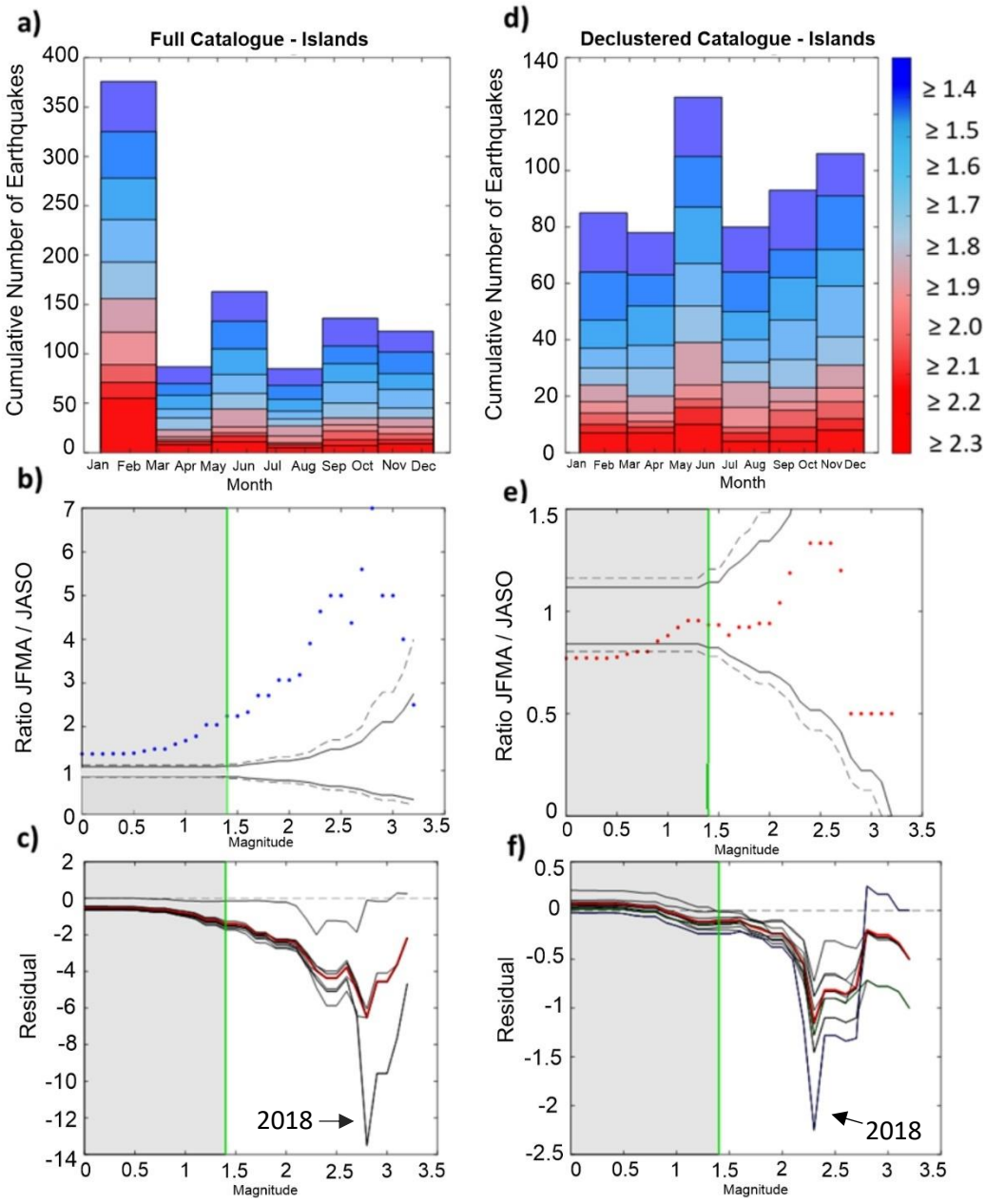

Figure 23. **(a)** Histogram for the islands seismicity of the Azores stacked on an annual timescale (divided into 2-month bins) between 1 January 2008 and 31 December 2018. The colors on the histogram indicate the magnitude cut-off used in each case. **(b)** Observed ratio (blue dots) of the number of earthquakes occurring in January, February, March, April (JFMA), to those occurring in July, August, September, October (JASO) as a function of cut-off magnitude. Grey shaded areas indicate the magnitude of completeness 1.4. Dashed and solid black lines indicate the 99% and 95% confidence limits, respectively. **(c)** Residuals of the Jack-Knife analysis. The black lines indicate the residual at each magnitude band between the calculated ratio and the 95% confidence limit. The ratios are calculated for

the same catalogue but removing each calendar year of the data. The red line represents the residuals of the observed ratio (the blue/red dots shown in **c, d)**. The black arrow highlights the different pattern of the year 2018. The confidence limits are estimated independently for each test. **d–f** are as **a–c**, but for the declustered seismic catalogue.

The full catalogue presented high tendency for seismicity in January and February, while the declustered catalogue presented more earthquakes in May and June, over 11 years (Figure 23a, d). To test the statistical significance of this observation, the cut-off magnitude was varied and the ratio of events occurring in JFMA to those occurring in JASO was computed (Figure 23b, e).

The ratio JFMA/JASO is higher than 1 for the full catalogue, which indicates more events happening in JFMA than in JASO. But after the declustering we see that more events are happening in late summer (JASO). Then the observation was tested against the possibility of observing a similar ratio by chance, by computing the 95% and 99% confidence limits of the 10.000 random seismic catalogues. However, the seasonality was not confirmed to be genuine for the declustered catalogue, since events above the magnitude of completeness ($M > 1.4$) lie within the 95% and 99% confidence limits, which means that there is a possibility of a similar ratio happen by chance. Unlike the declustered catalogue, the ratio in the full catalogue (where the earthquakes are clustered) does not lie inside the confidence limits, and follows a pattern different from the New Madrid Seismic Zone, in which the ratio is lower than 1. The values higher than 1 indicate that more events are happening in winter than in summer.

The Jack-Knife analysis was applied to the data to identify if different behaviors are present over the years and influencing the seismicity, such as extreme climate events. Moreover, according to Craig et al. 2017 despite declustering the catalogue there is a possibility of the seasonal trend being influenced by a small number of extreme deviations, rather than an overall trend.

The Jack-Knife analysis applied to the full catalogue indicates a different behavior during the year of 2018, shown in the residuals plot (Figure 23c, f) and in the ratios JFMA/JASO plot (Figure 24), in the analysis of the full catalogue.

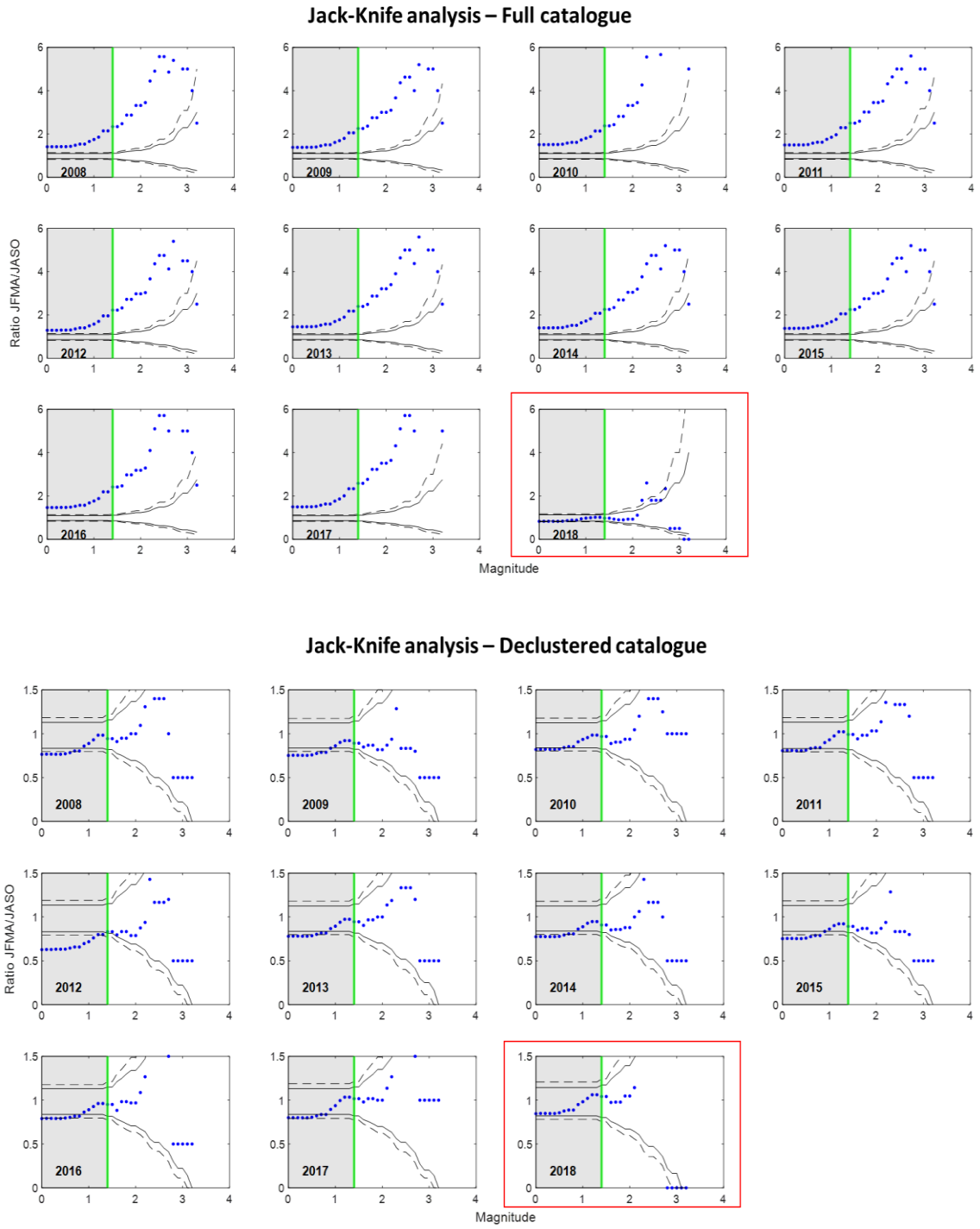

Figure 24. Results of the complete Jack-Knife analysis for the full and declustered Azores (islands) catalogues. Blue dots are the observed ratio of the number of earthquakes occurring in the four-month period JFMA (January, February, March, April) to those occurring in JASO (July, August, September, October) as a function of cut-off magnitude. Grey rectangle indicates the magnitude of completeness 1.4.

Solid and dashed lines represent the 95% and 99% confidence limits estimated independently for each test. The number in the lower left corner of each panel indicates the year of data removed from January 2008 to December 2018 overall time period. Red rectangle highlights the different behavior of the ratio when removing 2018 from the data.

Figure 24 shows that the data is influenced by extreme events that happened in 2018. In February 2018 there was a high seismic activity recorded in São Miguel Island, which interfere in the data statistics. Therefore, the results of the Jack-Knife suggest a genuine seasonality for the full catalogue from 2008 to 2017, while the declustered catalogue indicates that the seasonality is not genuine, confirmed by all ratios that lie inside the confidence limits.

6.2 SEASONAL VARIATIONS IN THE AZORES OCEAN SEISMICITY

Repeating the same processes of the islands catalogue, the earthquake frequency for the ocean seismic activity was plotted to observe seasonal patterns. Unlike the islands, the earthquake frequency for the ocean shows an apparent seasonality over the 11 years, which is clearer in the declustered data (Figure 25a, b). The cumulative rates increase over the years, which may be related to improvements in the seismic networks. The declustering process removed jumps between 2015 and 2016, shown in the detrended residuals plot (Figure 25c).

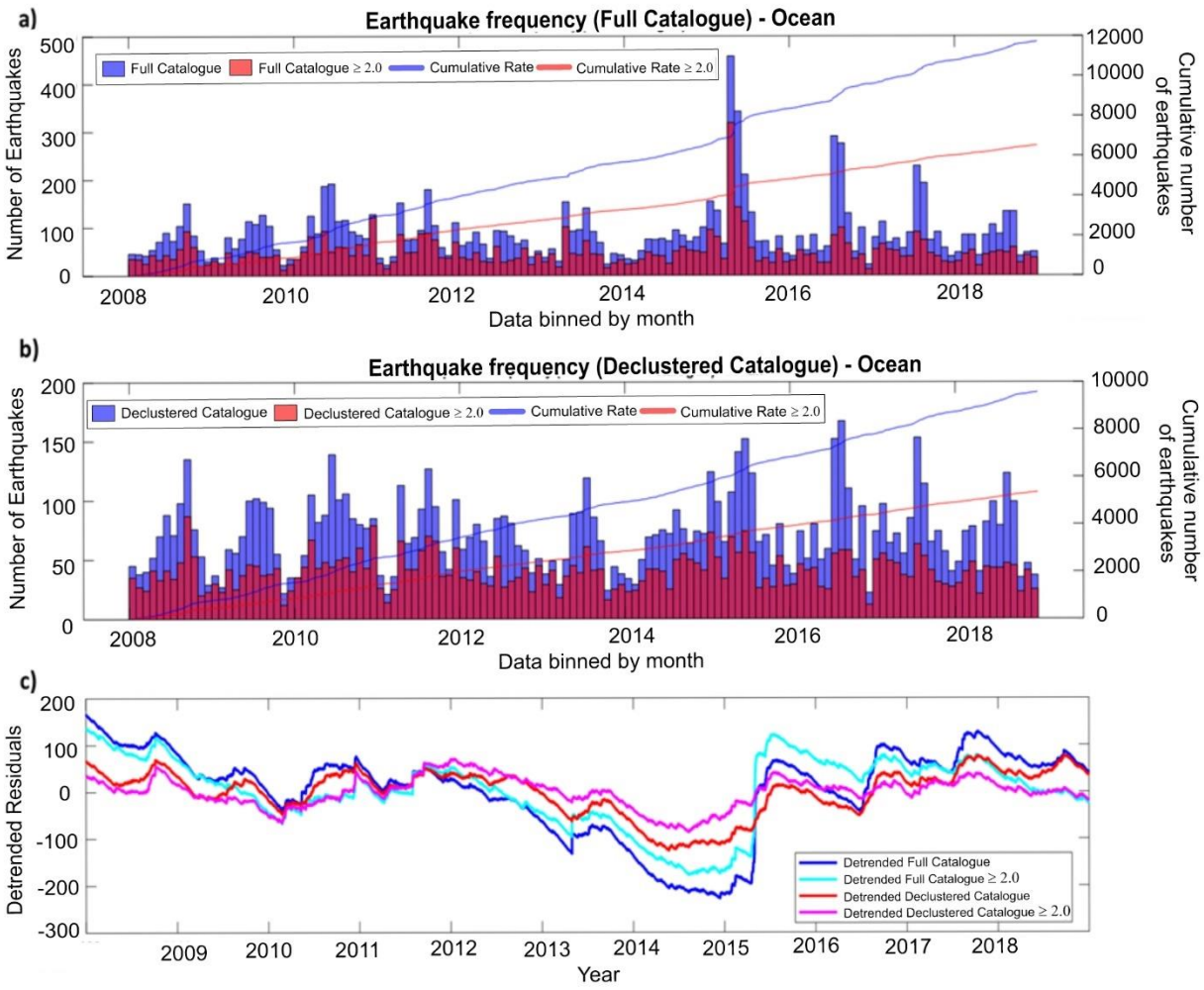

Figure 25. **(a)** Histogram frequency distribution for the full Azores ocean catalogue (Blue) and considering only earthquakes >= M2.0 (Red), and their respective cumulative rates. **(b)** is like **(a)** but for the declustered catalogue. **(c)** Cumulative number of earthquakes with a best-fit linear trend removed. Detrended residuals for the full catalogue (Dark blue), detrended full catalogue M >= 2.0 (Light blue), detrended declustered catalogue (Red), detrended declustered catalogue M >= 2.0 (Magenta).

Figure 26a-f show the analysis of seasonal trends in the Azores ocean seismicity. The histograms of the annual stacked data (divided into 2-month bins, Figure 26a, d) show a high tendency for seismicity in summer, mainly during July and August, when the cumulative number of earthquakes is higher than 1.000.

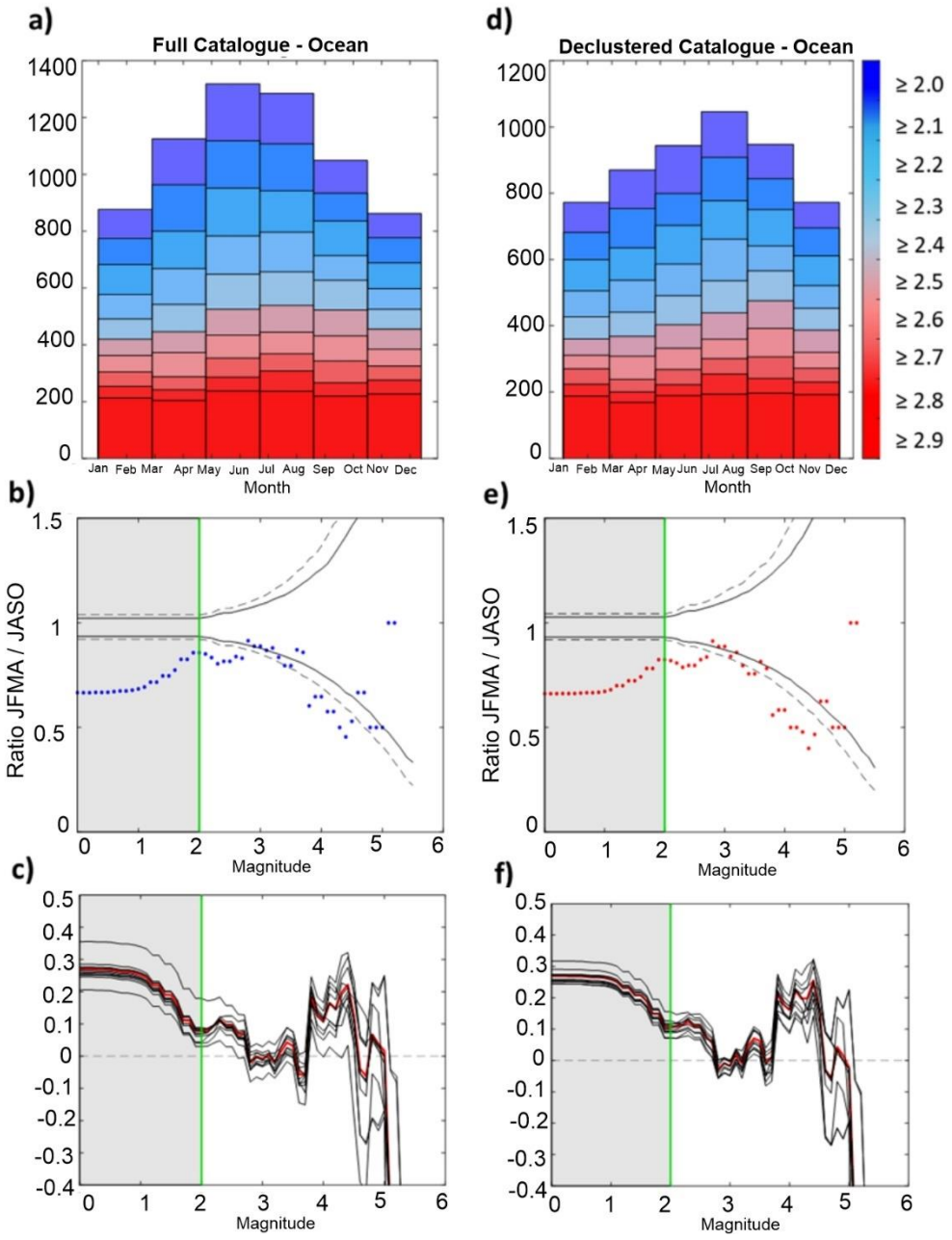

Figure 26. **(a)** Histogram for the ocean seismicity of the Azores stacked on an annual timescale (divided into 2-month bins) between 1 January 2008 and 31 December 2018. The histogram colors indicate the magnitude cut-off used in each case. **(b)** Observed ratio (blue dots) of the number of earthquakes occurring in January, February, March, April, to those occurring in July, August, September, October as a function of cut-off magnitude. Grey shaded areas indicate the magnitude of completeness 2.0. Dashed and solid black lines indicate the 99% and 95% confidence limits, respectively. **(c)** Residuals of the Jack-Knife analysis. The black lines indicate the residual at each magnitude band between the calculated ratio

and the 95% confidence limit. The ratios are calculated for the same catalogue but removing each calendar year of the data. The red line represents the residuals of the observed ratio (the blue dots shown in **c, d)**. The confidence limits are estimated independently for each test. Positive values are those where the magnitude bands exceed the confidence limits in **b**. **d–f** are as **a–c**, but for the declustered seismic catalogue.

The ratio of events occurring in January, February, March and April (JFMA) to those occurring in July, August, September, and October (JASO) was calculated, as well as the 95% and 99% confidence limits of the random seismic catalogues (Figure 26b, e), in order to test if it is possible to observe a low ratio between JFMA and JASO by chance. Unlike the islands, the ratio JFMA/JASO remains lower than 1 in the full and declustered data, just like the New Madrid Seismic Zone, which means more events happening in summer (JASO) than in winter/spring (JFMA).

Figure 26b, e show that mostly between M2.0 (the magnitude of completeness) and M2.7, and between M3.8 and M4.5 the probability that the observed low ratio would be due to chance is less than 1% in both cases (full and declustered data), for specific magnitude bands. For magnitude bands M > 5, the number of earthquakes is insufficient to provide a statistically significant trend. According to Bollinger et al. 2007, at such high magnitudes, purely instrumental effects are unlikely to produce an artificial seasonality, therefore the observed seasonality is genuine.

Knowing that the seasonality is genuine, the Jack-Knife analysis was applied to the data to confirm the genuineness and to identify different behaviors over the years.

The residuals of the Jack-Knife analysis (Figure 26c, f) exclude the possibility of extreme events over the years that could influence the seismicity. Thus, the exclusion of each year of data separately from the data series does not result in any of the remaining catalogues not having a statistically significant seasonal variation between the JFMA and JASO periods.

The positive values in Figure 27c, f are those where the magnitude bands exceed the confidence limits in Figures 26b, e.

Figure 27 shows the results of the Jack-Knife analysis after the exclusion of the years.

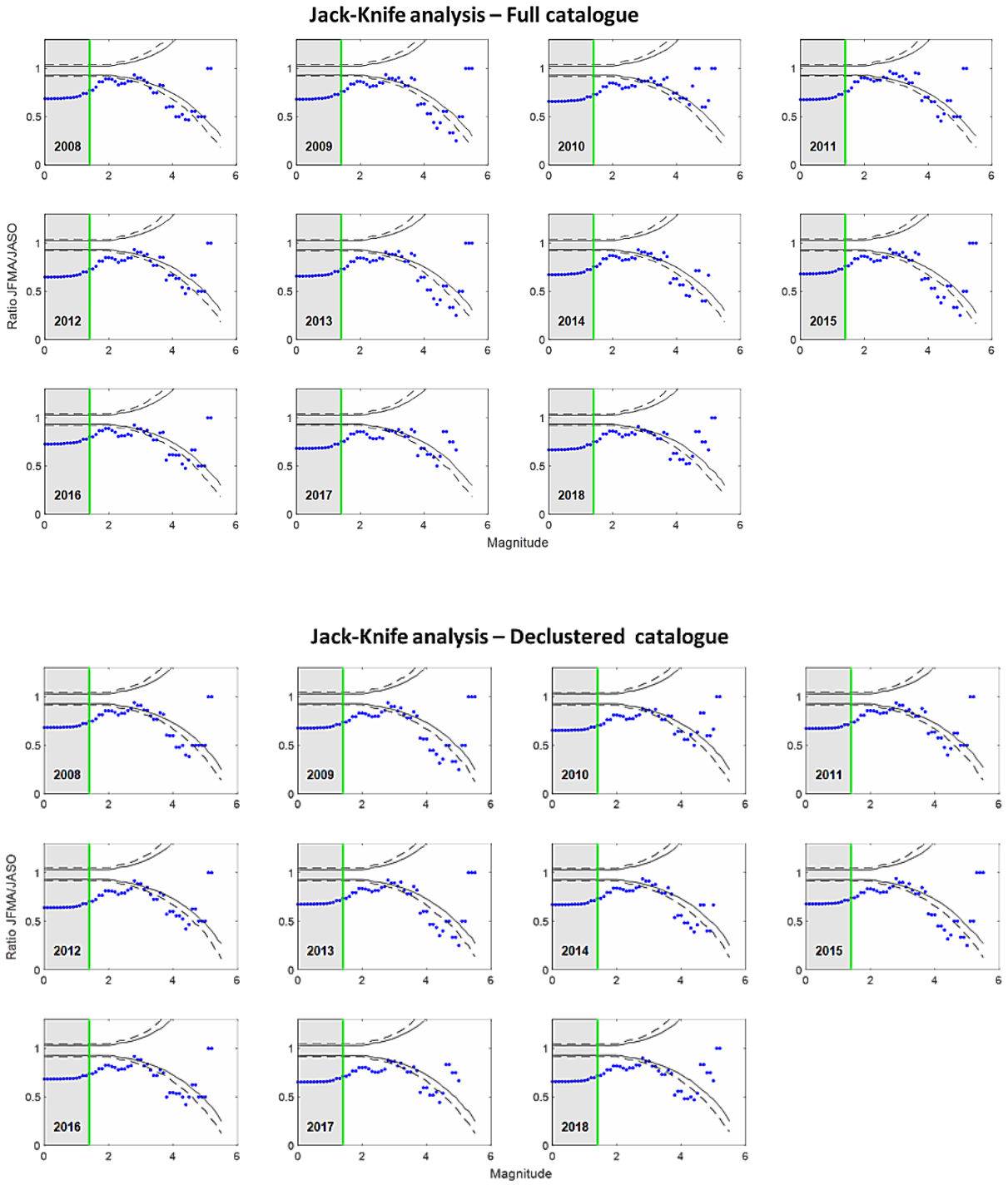

Figure 27. Results of the complete Jack-Knife analysis for the full and declustered Azores (ocean) catalogues. Blue dots are the observed ratio of the number of earthquakes occurring in the four-month period JFMA (January, February, March, April) to those occurring in JASO (July, August, September, October) as a function of cut-off magnitude. Grey rectangle indicates the magnitude of completeness 2.0.

Solid and dashed lines represent the 95% and 99% confidence limits estimated independently for each test. The number in the lower left corner of each panel indicates the year of data removed from the 1 January 2000 to 31 December 2015 overall time period.

Unlike the ratios calculated for the islands seismicity data, the ocean ratios follow a similar pattern over the years. Therefore, the apparent seasonality for the Azores ocean seismicity was considered genuine and not influenced by extreme events.

6.3 CORRELATION WITH ATMOSPHERIC AND HYDROLOGIC TIME SERIES

The monthly times series of the Rainfall, Atmospheric and Mean Sea Level Pressure and the Significant Height of combined wind waves and swell (which is the combined height of the sea and the swell, known as the total wave height or significant wave height), obtained from the ERA5 grid were used in the correlation with the seismicity rate, calculated using the Azores ocean declustered data, to investigate if they were related.

The five first components of each time series given by the Singular Spectrum Analysis were chosen to be correlated with the five first components of the ocean seismicity rate, since these components explain most of the signal (> 60%), as shown detailed in section 4.5, Figure 14.

The ocean seismicity rate is negatively correlated with the rainfall (-0.69) and with the significant height of combined wind waves and swell (-0.77) (Table 1). On the other hand, the atmospheric pressure and the mean sea level pressure are positively correlated with the ocean seismicity rate, presenting +0.40 and +0.39 correlation coefficients, respectively, shown in Figure 28a-d. No lags were observed between the correlated time series.

The overall results of the correlations are summarized in Table 1. Furthermore, to confirm if the results of the correlations are significant the t-student test (Table 1) was performed considering a two-tail significant test with a 95% significance level. The null hypothesis (H_0) is rejected when the $t_0 > \mathrm{t(df)}$ or $t_0 < -\mathrm{t(df)}$, which means that the correlation coefficient is significant.

a)

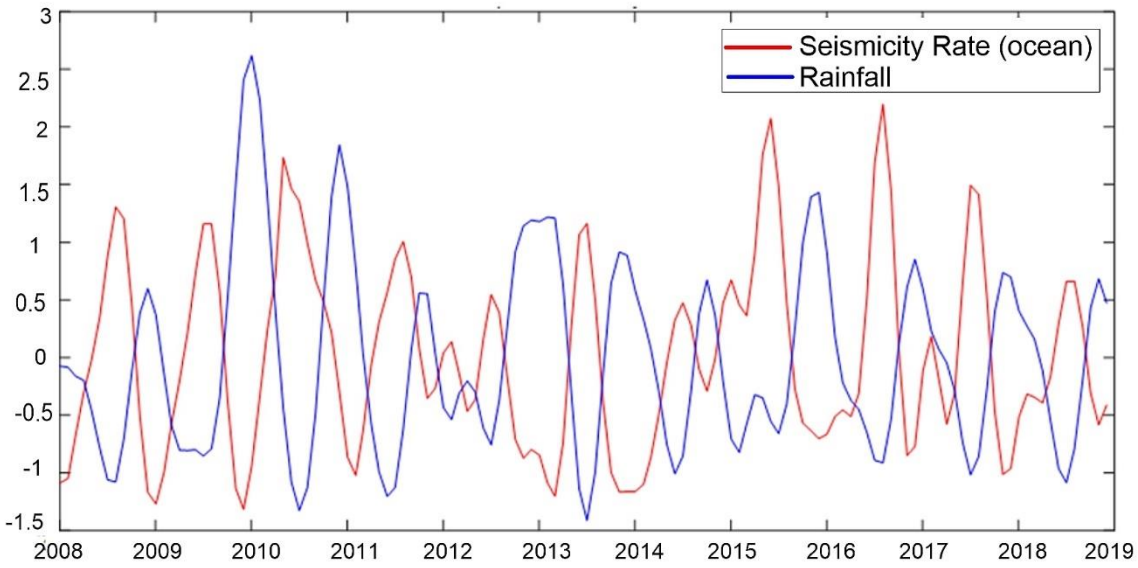
Seismicity rate vs Rainfall
Seismicity Rate (ocean)
Rainfall
3
2.5
2
1.5
1
0.5
0
-0.5
-1
-1.5
2008
2009
2010
2011
2012
2013
2014
2015
2016
2017
2018
2019

b)

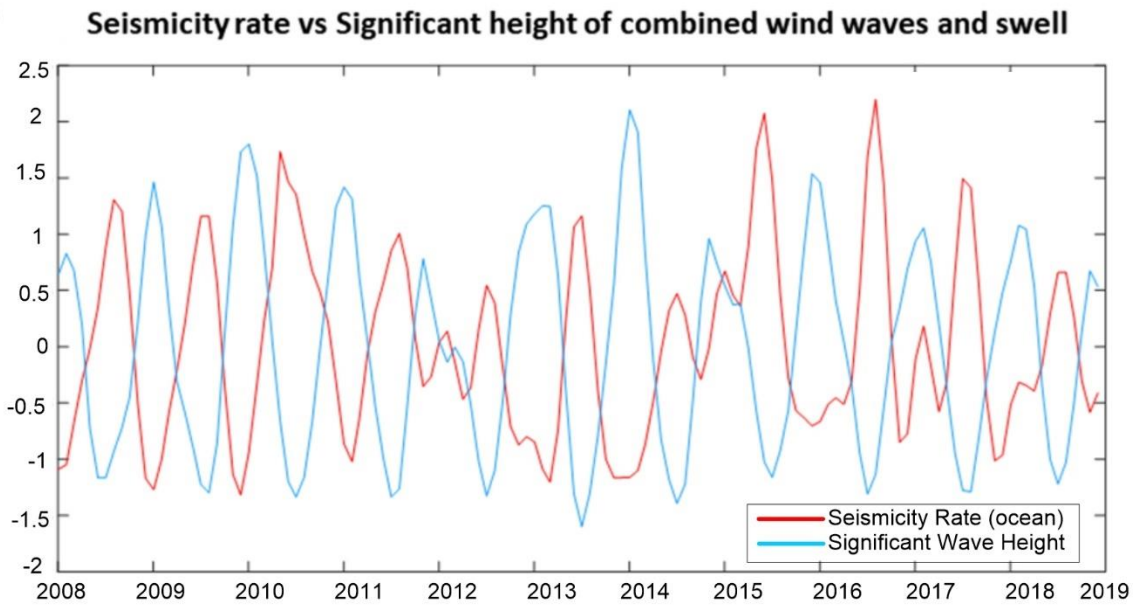
Seismicity rate vs Significant height of combined wind waves and swell
Seismicity Rate (ocean)
Significant Wave Height
2.5
2
1.5
1
0.5
0
-0.5
-1
-1.5
-2
2008
2009
2010
2011
2012
2013
2014
2015
2016
2017
2018
2019

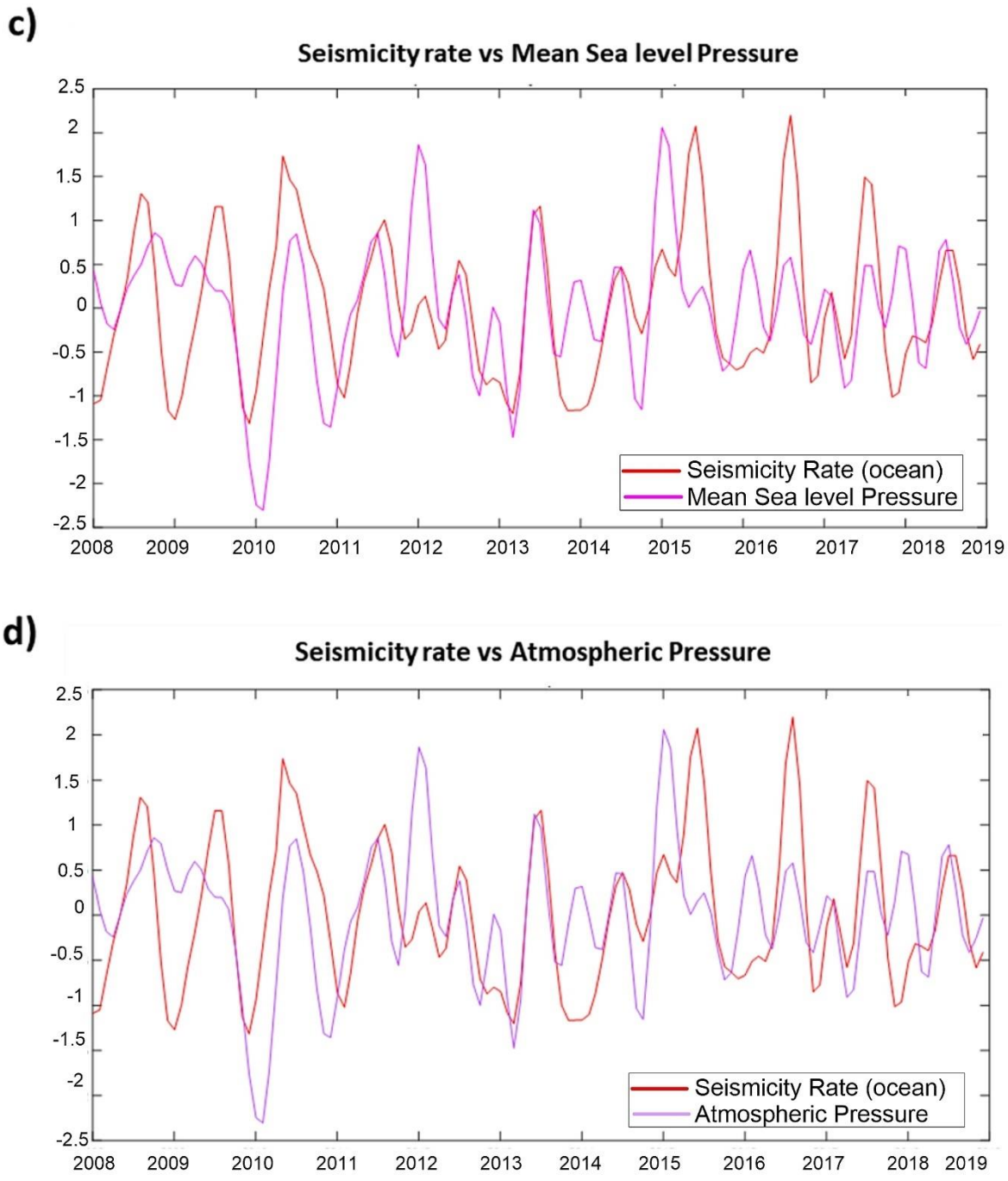

Figure 28. Results of the correlation between the Ocean seismicity rate (red line) and the **(a)** Rainfall, **(b)** Significant Height of combined wind waves and swell, **(c)** Atmospheric and **(d)** Mean Sea level Pressure monthly time series.

Table 1. Results of the correlation between the Ocean seismicity rate and the Significant Height of combined wind waves and swell, Rainfall, Atmospheric Pressure and Mean Sea level Pressure monthly time series, and the t-student test.

Time series	Correlation Coefficient	t-student test			
		t-statistic (t_0)	*t-critical lower*	*t-critical upper*	*Null hypothesis*
Ocean Seismicity Rate vs. Significant height of combined wind waves and swell	-0.77	-5.6	-2.06	2.06	rejected
Ocean Seismicity Rate vs. Rainfall	-0.69	-4.38	-2.06	2.06	rejected
Ocean Seismicity Rate vs. Atmospheric Pressure	0.4	2.21	-2.04	2.04	rejected
Ocean Seismicity Rate vs. Mean sea level Pressure	0.39	2.21	-2.04	2.04	rejected

*The Ocean Seismicity Rate was calculated using the ocean declustered data.
***The Null hypothesis is rejected when** $\boldsymbol{t_0 > t(df)\ or\ t_0 < -t(df)}$

As shown in Table 1, the correlations with the significant wave height and the rainfall presented the t-statistic lower than the t-critical lower, while the atmospheric pressure and mean sea level pressure presented the t-statistic higher than the t-critical upper. In all cases, the null hypothesis was rejected, which means the correlations are significant.

Next, the correlations were repeated for all time series. But this time using the ocean seismicity rate, calculated using the declustered data above the magnitude of completeness (M2.0).

When considering only earthquakes above M2.0, the correlations with the atmospheric and mean sea level pressure were not significant. The rainfall and the significant wave height, continue to present a negative correlation with the ocean seismicity rate, but now with a lower coefficient: -0.35 and -0.45, respectively, but still significant as confirmed by the t-student test: -2.19 < -2.02 for rainfall, and -3.06 < -2.02 for significant wave height.

7 DISCUSSION

The ocean seismicity rate (calculated using the ocean declustered data) presented a strong significant anti-correlation mainly with the rainfall and the significant height of combined wind waves and swell time series. Figure 29 shows 11 years of the time series, their most significant principal components, and the annual stacked data.

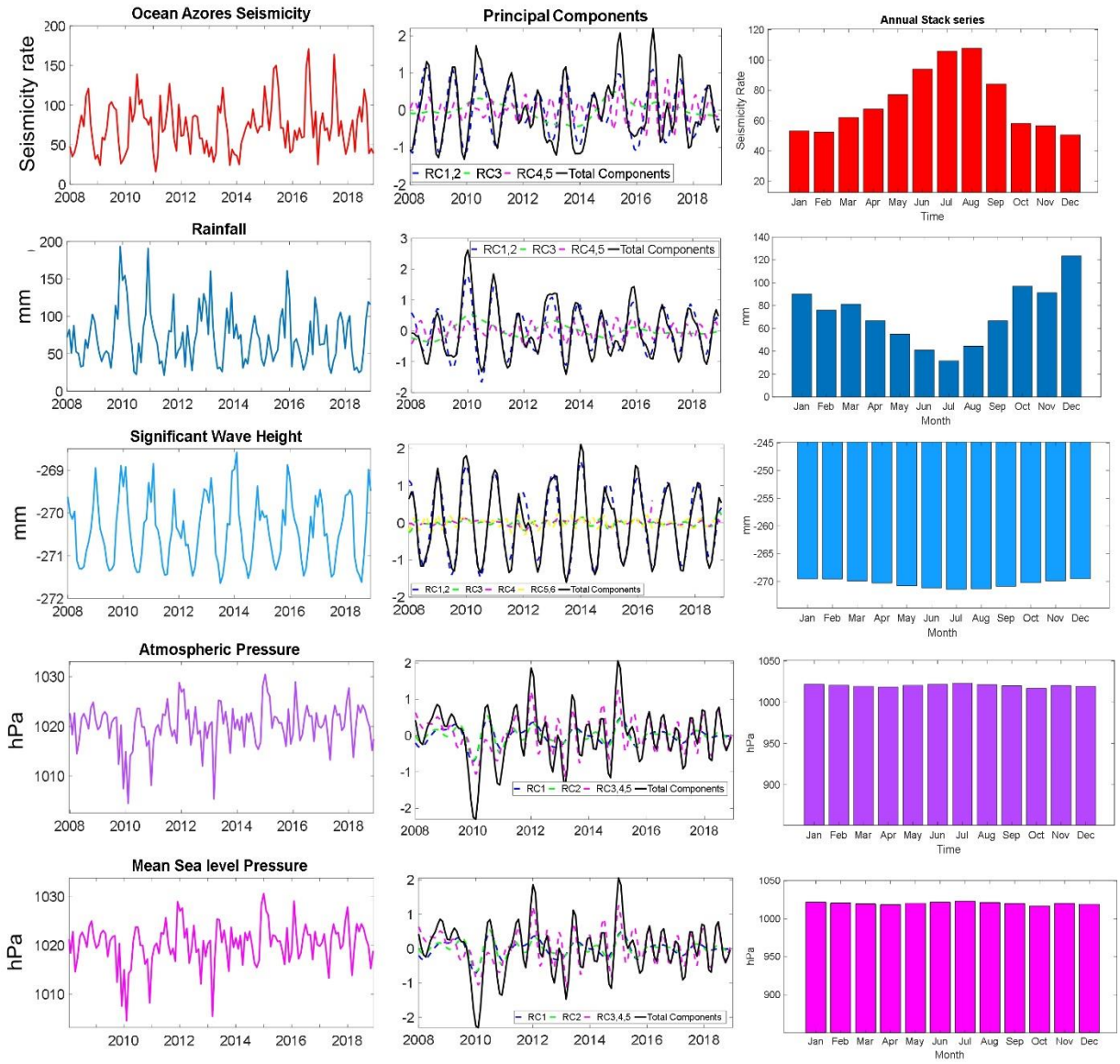

Figure 29. Ocean seismicity rate (solid red line), Rainfall (solid dark blue line), the Significant Height of combined wind waves and swell (solid light blue line), Atmospheric (solid purple line) and Mean Sea level Pressure (solid magenta line) time series. The sum of their 5 first reconstructed components (solid

black line), and the components that were summed up (colorful dashed lines). Components pair are shown combined. The data stacked on an annual time scale is represented by the histograms. The stacked data for the atmospheric and mean sea level pressure does not start at 0 (y-axis) to capture better the pressure behavior over the months.

When comparing the time series each other and the sum of their principal components (solid black line), we see that every peak in the ocean seismicity rate corresponds to a valley in the rainfall time series and to a valley in the significant wave height. Moreover, the correlation between the rainfall and the significant wave height is +0.80, confirmed to be significant by the t-student test (5.81 > 2.08).

Component pair 1 and 2 (blue dashed line) of the seismicity rate, rainfall and significant wave height represent an oscillation of annual period, while component 3 is a multi-annual trend. The atmospheric pressure and mean sea level pressure present both 18.8 months period in the first component, which influenced the results of the correlation. The annual signal (RCs 1 and 2) also shows the same anti-correlation between the seismicity, rainfall and the significant wave height, as well as the multi-annual signal (RC 3) of the seismicity and the rainfall.

The stacked data (histograms) makes clear the anti-correlation over 11 years, between the ocean seismicity rate, which is higher during the summer, mainly in July/August, the rainfall and the significant wave height, which are lower in the same months.

The atmospheric pressure and mean sea level pressure did not show a strong correlation with seismicity, as mentioned at the previous section, and are not easily observed in the principal components plots, although in the stacked data we see a very smooth increase of the pressure during summer months.

As mentioned previously, an anti-correlation with the rainfall and the significant wave height was also found when calculated the ocean seismicity rate using the declustered data above the magnitude of completeness 2.0, but this time with a lower coefficient. It is important to understand that when we consider the magnitude of completeness (Mc) of a catalogue, it might not reflect the reality for the whole area, since the Mc varies with the area and the time. Therefore, for M > 2.0 the correlation is not as good as it was when considering all magnitudes.

Considering these results, we see that when the rainfall and the height of the sea and the swell (significant height of the waves) increase, the ocean presents a lower seismicity rate, and is the lowest during the winter/spring months. The seismicity rate increases during the summer, when the rainfall and the wave height fall.

The results obtained here for the ocean follow the pattern of the New Madrid Seismic Zone obtained by Craig et al. 2017, in which during the rainy season the seismicity rate falls. During the wet season, when the crust is suffering with the water load, the subsidence movement occurs, and less earthquakes are registered, while during the dry season (summer), the crust rebounds since the water load is released, triggering the faults and generating a high number of earthquakes.

As exemplified in section 2, Figure 3, besides the rainfall and the river stage time series, Craig et al. 2017 used GPS vertical displacements observations that show a strong annual variation linked to the redistribution of continental water masses in the Mississippi basin over the year (Craig et al. 2017), as well as GRACE measurements that show a strong annual signal in regions of large hydrological load change.

The surface-loading variations, obtained from GRACE was used in a spherical layered elastic Earth model to calculate the strain and stress fields responses to the variations in the continental water mass, and compared to the GPS displacements, showing a good match. In addition, the calculated strain and stress fields was used to estimate the Coulomb stress that is used quantify the susceptibility of the NMSZ fault to failure under annual surface loading. The Coulomb stress is positive in tension, which means that an increase in this parameter indicates enhanced seismicity in the area. The authors found a variation of 1 kPa over each yearly cycle, which is influencing the seismic activity in the NMSZ.

The dominant controlling mechanism on the NMSZ appears to be variations in the normal stress. Moreover, due to little or no time delay between the hydrological variations and the seismicity rate, the authors concluded that the stresses are exerted directly in the fault plane. On the contrary, in Nepal Himalaya, according Bettinelli et al. 2008, a phase lag between the seasonal strain and stress variations (around 2–4 kPa), induced by water storage variations, that is

helping to drive seasonal variations in the seismicity, are assigned to high pore pressure effects, and the presence of fluids in the area.

Although no phase lag was found between the Azores ocean seismicity rate and the hydrological/atmospheric time series, unlike the New Madrid Seismic Zone and the Himalaya, where the authors found the controlling mechanism that is acting on the faults, in the Azores case, it is still not possible to suggest that no phase lag indicates that the stresses are being exerted directly on the faults, since deeper investigations must be done to understand how the studied hydrological loads interact to the oceanic crust to trigger the seismicity in the archipelago.

At first, there was a suspicion that the high tendency for seismic activity in summer would be due to the ocean background noise, since the capacity of the network to record the earthquakes, during winter months is reduced, when the ocean is more agitated. This possibility was excluded since the ocean background noise is not capable of mask higher magnitudes around M4.0, which showed a genuine seasonality in the ocean. Being the background noise a regional signal, it should interfere in the islands as well, which did not happen.

As mentioned in section 6.1, Figure 24, the Monte Carlo simulation showed that seasonality of the islands is not genuine when considering the declustered catalogue, which might be linked to the extreme events found in 2018. The pattern of the ratios observed in the full catalogue (Figure 24) indicates a genuine seasonality for all years, except for 2018, and show that more events are happening in winter than in summer, unlike the results found for the ocean. The fact that the full catalogue presents a genuine seasonality and the declustered does not, suggests that the seasonality happens in the seismic clusters, which are a group of earthquakes that happen together in time (eliminated during the declustering process). The seismic clusters are associated to the hydrothermal activity (Petrosino et al., 2018) and to the percolation of fluids on the crust (e.g., rainfall).

7.1 LIMITATIONS AND FUTURE DIRECTIONS

It is important to consider that although the ocean seasonality is genuine in the Azores seismicity rate, the strong correlation found between the rainfall and the significant wave height with the seismicity rate might be a coincidence of the natural cycles.

Further studies would be needed to investigate how exactly these mechanisms are impacting the seismic activity in the oceanic crust. As a continuation of this work, I highlight that it is crucial to calculate the stress and strain variations exerted by the water column, and compare the results with the ocean and islands seismicity rate, in order to know if the hydrological load is triggering the seismicity. In some cases, as seen by Bettinelli et al. 2008 work, the seismicity rate does not correlate directly with the hydrological loads, but with the strain and stress variations caused by them.

Other possible mechanisms that interfere in the ocean, should be investigated in its relationship with seismicity, such as the tides. The Solid and ocean Earth tides have been evoked to influence the seismicity and volcanic eruptions in a variety of places around the world, like in Italy, Iceland, and Hawaii, since a rising sea-level corresponds to a larger ocean loading on the volcanic system, resulting in the extrusion of magma (Custódio et al. 2003; Sottili & Palladino 2012; Scholz et al. 2019; Dumont et al. 2020; Dumont et al. 2021). Tidal stresses beneath the oceans can be up to an order of magnitude higher than those found in the continents because of the effects of loading by ocean tides (Wilcock 2001). The loading exerted by the water column in the crust can be explained by the hydrostatic state of stress wherein pressure forces are exerted equally in all directions and pressure increases proportionately with depth (Turcotte & Schubert 2014).

Some studies about the mechanism of tidal triggering of earthquakes in magmatic areas at mid-ocean ridges have shown that tidally-induced stresses within the subseafloor modulate both fluid flow and microearthquake origin times by generating pore pressure changes (Tanaka 2002; Tolstoy 2002; Wilcock 2009; Stroup et al. 2009; Scholz et al. 2019). Moreover, it was already evidenced an increase in the earthquake frequency during the low tide, due to the tidally induced inflation of the magma chamber that happens when there is a reduction of the vertical stress, in low tides (Wilcock 2001; Scholz et al. 2019).

As a first approach, all the 9 islands in this work were analyzed together, which might be a reason for no genuine seasonality to be found in the declustered catalogue. Another reason is the size of the sampling. The islands catalogue has 1.773 events while the ocean presents 11.719 events, resulting in robust results. Moreover, different processes might be occurring in both places that lead to the different results. Then for future studies, I suggest repeating the steps of this work but now focusing in one of the islands, and use time series from local stations. In 2009 the seismicity rate (from 2003 to 2004) around the Fogo massif in São Miguel Island was suggested to be triggered by the rainfall due to their good correlation, possibly through pressure changes at depth in response to surface rain and/or an interaction with the geothermal system (Martini et al. 2009).

In addition, look for the relationship of the seismicity rate with new time series, such as groundwater variations and surface displacement, as well as tide effects would be a good contribution and will bring new results. In São Miguel island, Jónsson et al. 1999 analyzed GPS displacements and found periods of inflation and deflation in the area, indicating slight deflation of the volcano, that might be due to pressure decrease in a shallow magma chamber beneath Fogo. We need to consider that the deflation/inflation of the chamber might be due to the earth tides effect, that influence the volcanic system, as seen in the aforementioned studies (Dumont et al. 2020; Dumont et al. 2021).

8 CONCLUSION

This work evidenced seasonal modulation of the oceanic seismicity in the Azores, correlated with atmospheric and hydrological variations.

The results of the New Madrid Seismic Zone similar to Craig et al. 2017 results confirm the reliability of the methodology that was applied to the Azores data.

The declustering of the Azores catalogue, defined from 2008 to 2018 helped to remove jumps from the data, coming from the clusters (foreshocks and aftershocks), maintaining only the independent events for the analysis. The Azores catalogue divided into islands earthquakes and ocean earthquakes show that unlike the ocean, the islands did not present a genuine seasonality for both catalogues, only for the full one from 2008 to 2018, which is probably linked to extreme events in 2018. The seasonality found in the clusters may suggest that the percolation of fluid or the hydrothermal activity in the islands are triggering the seismicity, since the clusters are associated with them. According to some studies, a high foreshocks/aftershocks productivity, are generally attributed either to a cascade of elastic fault rupture or to the hidden influence of fluids, particularly in volcanic areas and on transform faults (Vidale & Shearer 2006).

The ocean earthquakes catalogue presented a seasonality over 11 years, confirmed to be genuine by the statistical methods for both declustered and full catalogues from 2008 to 2018. The Azores ocean seismicity behaves similar to the New Madrid Seismic Zone. The annual stacked data demonstrates that for 11 years there is a high tendency for more earthquakes to happen in summer, mainly during July and August, for magnitudes range from M2.0 to M2.7 and from M3.8 to M4.5. The results obtained here point to a possible role played by the rainfall and the significant wave height in triggering the ocean seismicity, due to the strong anti-correlation found. Further studies are encouraged in order to quantify the strain and stresses exerted on the crust by the ocean load (affected by the rainfall and wave height) and compare it with the results obtained here. If the ocean load presented an annual variation, it might be a reason for the ocean seismic activity.

This work provides an assessment of cyclical variations in seismicity and their relationship with hydrological and atmospheric disturbances in the Azores region, and a first approach of rainfall

and significant wave height as possible mechanisms that interfere in the ocean load and trigger the ocean seismic activity in the region. The study contributes to improving our understanding about the earthquakes triggering mechanisms and the prediction of times of enhanced seismicity in volcano-tectonic active systems.

REFERENCES

Adam C., Madureira P., Miranda J.M., Lourenço N., Yoshida M., and Fitzenz D. (2013). Mantle dynamics and characteristics of the Azores Plateau. Earth and Planetary Science Letters, 362, 258-271.

Bettinelli P., Avouac J-P., Flouzat M., Bollinger L., Ramilien G., Rajaure S., and Sapkota S. (2008). Seasonal variations of seismicity and geodetic strain in the Himalaya induced by surface hydrology. Earth Planet. Sci. Lett. 266, 332–344.

Bollinger L., Perrier F., Avouac J. P, Sapkota S., Gautam U., and Tiwari D. R. (2007). Seasonal modulation of seismicity in the Himalaya of Nepal. Geophysical Research Letters, 34.

Borges J. F., Bezzeghoud M., Buforn E., Pro C., and Fitas A. (2007). The 1980, 1997 and 1998 Azores earthquakes and some seismo-tectonic implications. Tectonophysics, 435, 37-54.

Broomhead D.S. & King G.P. (1986). Extracting qualitative dynamics from experimental data: Physica D: nonlinear phenomena, 20, 217–236.

Brothers D., Kilb D., Luttrell K., Driscoll N., and Kent G. (2011). Loading of the San Andreas fault by flood-induced rupture of faults beneath the Salton Sea. Nat. Geosci. 4, 486–492.

Craig T.J., Chanard K., andCalais E. (2017). Hydrologically-driven crustal stresses and seismicity in the New Madrid Seismic Zone. Nature Communications, 8, 2143.

CERI. New Madrid Earthquake Catalog (Centre for Earthquake Research and Information, Memphis, TN, USA). Available at http://www.memphis.edu/ceri/seismic/catalog.php. Accessed in 2021.

Csontos R. & Arsdale R. V. (2008). New Madrid seismic zone fault geometry, Geosphere, 4 (5), 802–813.

Custodio S. I. S., Fonseca J. F. B. D., d'Oreye N. F., Faria B. V. E., and Bandomo´ Z. (2003). Tidal modulation of seismic noise and volcanic tremor, Geophysical Research Letters, 30, 15, 1816.

Dickinson J.E., Hanson R.T., and Predmore S.K. (2014). HydroClimATe - Hydrologic and climatic analysis toolkit: U.S. Geological Survey Techniques and Methods 4-A9, 49.

Do Nascimento A. F., Cowie P. A., Lunn R. J., and Pearce R. G. (2004). Spatio-temporal evolution of induced seismicity at Açu reservoir, NE Brazil. Geophysical Journal International, 158, 1041–1052.

Dumont S., Le Mouëlc J. S., Courtillot V., Lopes F., Sigmundsson F., Coppola D., Eibl E. P .S., and Bean C. J. (2020). The dynamics of a long-lasting effusive eruption modulated by Earth tides. Earth and Planetary Science Letters, 5361, 16145.

Dumont S., Silveira G., Custódio F., Lopes F., Le Mouël J-F., Gouhier M., and Guéhenneux Y. (2021). Response of Fogo volcano (Cape Verde) to lunisolar gravitational forces during the 2014–2015 eruption. Physics of the Earth and Planetary Interiors, 312, 106659**.**

Fontiela J., Bezzeghoud M., Rosset P., Borges J. F., and Cota RodriguesF. (2014). Azores seismogenic zones. Comunicações Geológicas, 101(I), 29–35.

Fontiela J., Sousa Oliveira C., and Rosset P. (2018). Characterisation of Seismicity of the Azores Archipelago: An Overview of Historical Events and a Detailed Analysis for the Period 2000–2012. Kueppers U., Beier C. (eds) Volcanoes of the Azores. Active Volcanoes of the World. Springer, Berlin, Heidelberg.

ERA5. ECMWF – European Centre for Medium-Range Weather Forescasts. Available at https://www.ecmwf.int/en/forecasts/datasets. Accessed in 2021.

Gahalaut K., Gahalaut V. K., and Pandey M. R. (2007). A new case of reservoir triggered seismicity: Govind Ballav Pant reservoir (Rihand dam), central India. Tectonophysics, 439 (1–4), 171–178.

Gardine L. (2020). What is magnitude of Completeness? In Alaska Earthquake Center. Available at https://earthquake.alaska.edu/what-magnitude-completeness. Accessed in 2021.

Gaspar J.L., Queiroz G., Ferreira T., Medeiros A.R., Goular C., and Medeiros J. (2015). Earthquakes and volcanic eruptions in the Azores region: geodynamic implications from major historical events and instrumental seismicity. In: Gaspar, J.L., Guest, J.E., Duncan, A.M., Barriga, F.J.A.S., Chester, D.K. (eds.) Volcanic Geology of São Miguel Island (Azores Archipelago), Geological Society of London Memoir, 44, 33-49.

Gente P., Dyment J., Maia M., and Goslin J. (2003). Interactions between the MAR and the Azores hot spot during the last 85 Myr: emplacement and rifting of the hot spot-derived plateaus. Geochemistry Geophysics Geosystems, 4, 1-23.

Ghil M., Allen M.R., Dettinger M.D., Ide K., Kondrashov D., Mann M.E., Robertson A.W., Saunders A., Tian Y., Varadi F., and Yiou P. (2002). Advanced spectral methods for climatic time series: Reviews of Geophysics, 40, 1, 3-1–3-41.

Gutenberg B. & Richter C. F. (1944). Frequency of earthquakes in California. Bulletin of the Seismological Society of America, 34, 185–188.

Gruszczynska M., Rosat S., Klos A., Gruszczynski M., and Bohusz J. (2018). Multichannel Singular Spectrum Analysis in the Estimates of Common Environmental Effects Affecting GPS Observations. Pure Appl. Geophys., 175, 1805–1822.

Heki K. (2003). Snow load and seasonal variation of earthquake occurrence in Japan. Earth and Planetary Science Letters, 207, 159-164.

IPMA. Instituto Português do Mar e Atmosfera. Available at https://www.ipma.pt/pt/publicacoes/boletins.jsp?cmbDep=sis&cmbTema=bsi&idDep=sis&idTema=bsi&curAno=-1. Accessed in 2021.

Jónsson S., Alves M. M., and Sigmundsson F. (1999). Low rates of deformation of the Furnas and Fogo volcanoes, São Miguel, Azores, observed with the Global Positioning System, 1993–1997. J. Volcanol. Geotherm. Res. 92, 83–94.

Kreemer C. & Zaliapin I. (2018). Spatiotemporal Correlation Between Seasonal Variations in Seismicity and Horizontal Dilatational Strain in California. Geophysical Research Letters, 45, 9559–9568.

Luis J. F. & Neves M.C. (2006). The isostatic compensation of the Azores Plateau: A 3D admittance and coherence analysis. Journal of Volcanology and Geothermal Research, 156, 10–22.

Martini F., Christopher J. B., Saccorotti G., Viveiros F., and Wallenstein N. (2009). Seasonal cycles of seismic velocity variations detected using coda wave interferometry at Fogo volcano, São Miguel, Azores, during 2003–2004. Journal of Volcanology and Geothermal Research, 181, 231–246.

Neves M.C., Miranda J.M., and Luis J. F. (2013). The role of lithospheric processes on the development of linear volcanic ridges in the Azores. Tectonophysics, 608, 376–388.

Neves M. C., Cabral J., Luttrell K, Figueiredo P., Rockwell T., and Sandwell D. (2015). The effect of sea level changes on fault reactivation potential in Portugal. Tectonophysics, 658, 206–220.

Page M. T. & Hough S. E. (2014). The New Madrid Seismic Zone: Not Dead Yet. Science, 343 (6172), 762–764.

Pratt T. L. (1994). How Old is the New Madrid Seismic Zone? Seismological Research Letters, 65 (2): 172–179.

QGIS.org (2021). QGIS Geographic Information System. QGIS Association. Available at http://www.qgis.org. Accessed in 2021.

Reasenberg P. (1985). Second-Order Moment of Central California Seismicity, 1969-1982. Journal of Geophysical Research, 90, B7, 5479-5495.

Scholz C. H. (1968). The frequency-magnitude relation of microfracturing in rock and its relation to earthquakes. Bull. Seism. Soc. Am., 58, 399–415.

Scholz C. H, Tan Y. J., and Albino F. (2019). The mechanism of tidal triggering of earthquakes at mid-ocean ridges. Nature Communications,10, 2526.

Silva R., Carmo R., and Marques R. (2020). Characterization of the tectonic origins of historical and modern seismic events and their societal impact on the Azores Archipelago, Portugal. Geological Society, London, Special Publications, 501, 245-267.

Sottili G. & Plladino D. M. (2012).Tidal modulation of eruptive activity at open-vent volcanoes: Evidence from Stromboli, Italy. Terra Nova, 24, 233-237.

Stein R.S. (1999). The role of stress transfer in earthquake occurrence. Nature, 402, 605–609.

Stroup D. F., Tolstoy M., Crone T. J., Malinverno A., Bohnenstiehl D. R., and Waldhauser F. (2009). Systematic along-axis tidal triggering of microearthquakes observed at 9°50′N East Pacific Rise. Geophysical Research Letters, 36.

Tanaka S., Ohtake M., and Sato H. (2002). Spatio-temporal variation of the tidal triggering effect on earthquake occurrence associated with the 1982 South Tonga earthquake of Mw 7.5. Geophysical Research Retters, 29, 16.

Tanaka Y. (2014). An approximately 9-yr-period variation in seismicity and crustal deformation near the Japan Trench and a consideration of its origin. Geophys. J. Int. 196, 760–787.

Tolstoy M., Vernon F. L., Orcutt J. A., and Wyatt F. K. (2002). Breathing of the seafloor: tidal correlations of seismicity at axial volcano. Geology 30, 503–506.

Turcotte D. & Schubert G. (2014). Geodynamics. Third edition. United States of America, Cambridge University Press, New York.

Ueda T. & Kato A. (2019). Seasonal Variations in Crustal Seismicity in San-in District, Southwest Japan. Geophysical Research Letters, 46, 3172–3179.

United States Geological Service (USGS). Available at https://www.usgs.gov/natural-hazards/earthquake-hazards/science/new-madrid-seismic-zone?qt-science_center_objects=0#qt-science_center_objects

Vautard R., & Ghil, M. (1989). Singular spectrum analysis in nonlinear dynamics, with applications to paleoclimatic time series: Physica D 35, 395–424.

Vidale J.E. & Shearer P.M. (2006). A survey of 71 earthquake bursts across southern California: exploring the role of pore fluid pressure fluctuations and aseismic slip as drivers, J. geophys. Res. Solid Earth, 111(B5).

Warren N. W. & Latham G. V. (1970). An experimental study of thermally induced microfracturing and its relation to volcanic seismicity. Journal of Geophysical Research, 75(23), 4455–4464.

Wiemer S. 2001. A software package to analyze seismicity: ZMAP. Seismological Research Letters, 72(3), 373-382.

Wilcock W. S. D. (2001). Tidal triggering of microearthquakes on the Juan de Fuca Ridge. Geophysical Research Letters, 28, 3999-4002.

Wilcock W. S. D. (2009). Tidal triggering of earthquakes in the Northeast Pacific Ocean. Geophys. J. Int. 179, 1055-1070.

Wyss M. (1973). Towards a physical understanding of the earthquake frequency distribution. Geophys. J. R Astr. Soc., 31, 341-359.

ANNEX A. ANALYSIS OF SEASONAL TRENDS IN SEISMICITY AROUND THE NEW MADRID SEISMIC ZONE (NMSZ)

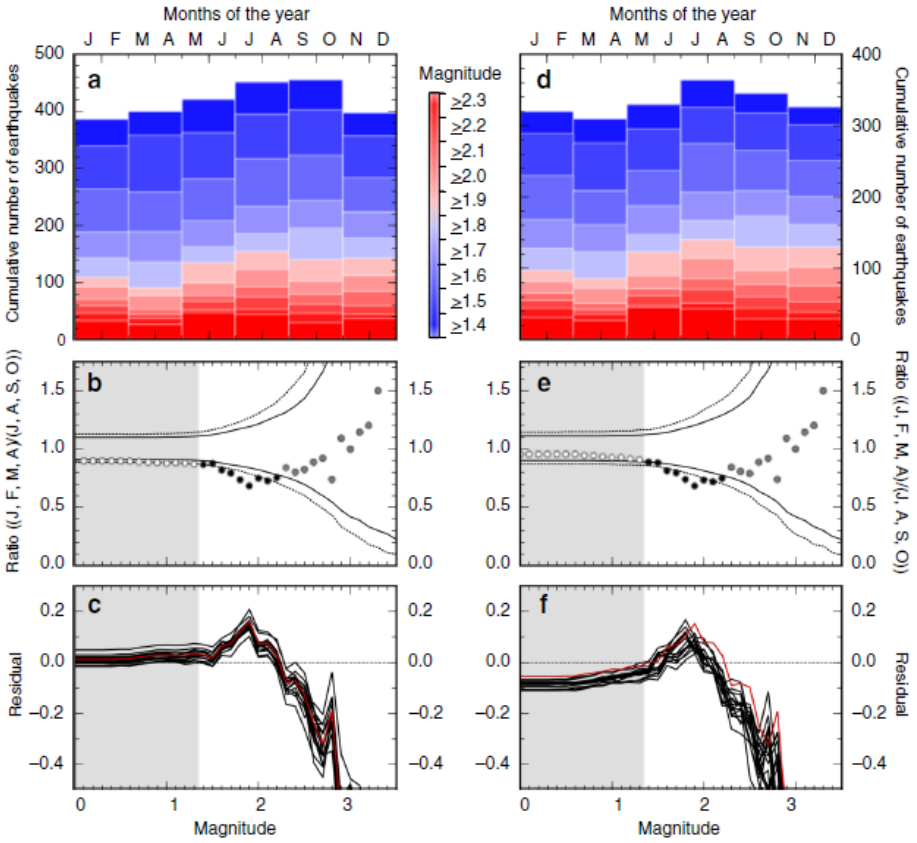

Figure 30. (a) Histogram (in 2-month bins) for the number of earthquakes in the complete catalogue between 1 January 2000 and 31 December 2015. Colors are indicative of the magnitude cut-off used in each case. **(b)** Ratio of the number of earthquakes occurring in the 4-month period encompassing January, February, March, April, to those occurring in July, August, September, October as a function of cut-off magnitude. Grey shaded areas indicate the magnitude of completeness. Dashed and solid black lines indicate the 99 and 95% confidence limits, respectively. Black points are those where the ratio exceeds the 95% confidence limit. **(c)** Results of a Jack-knife analysis of the seasonal trend. Lines indicate the residual at each magnitude band between the calculated ratio and the 95% confidence limit. Red line is for the full catalogue, as shown in **b**. Black lines are for the same catalogue with successive years of data removed. Confidence limits are estimated independently for each test **d–f** are as **a–c**, but for the seismicity catalogue after declustering (from Craig et al. 2017).

APPENDIX A. JACK-KNIFE ANALYSIS FOR THE FULL AND DECLUSTERED NEW MADRID SEISMIC ZONE CATALOGUE

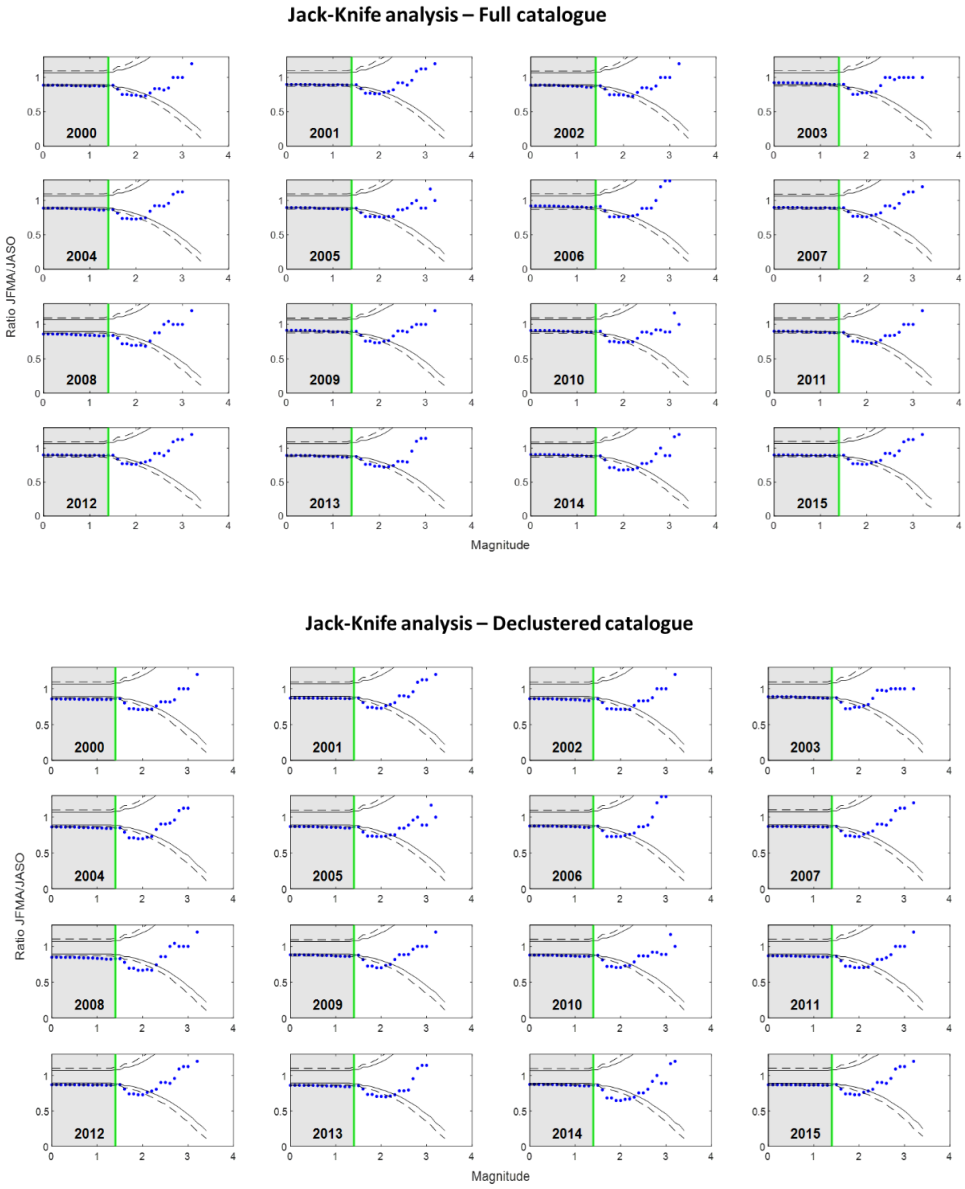

Figure 31. Results of Jack-Knife analysis for the full and declustered seismic catalogue (New Madrid Seismic Zone). Ratio of the number of earthquakes occurring in the four-month period encompassing January, February, March, April, to those occurring in July, August, September, October as a function of cut-off magnitude. Grey shaded areas indicate the magnitude of completeness 1.4. Number in the lower left corner of each panel indicates the year of data removed from the 1/1/2000 to 31/12/2015 overall time period.